Physics – Uspekhi **66** (9) 885 – 913 (2023)

REVIEWS OF TOPICAL PROBLEMS PACS number: 97.80.Jp

Generation of X-ray radiation in the inner regions of accretion disks around black holes, neutron stars, and white dwarfs

L G Titarchuk, E V Mikheeva, V N Lukash

DOI: https://doi.org/10.3367/UFNe.2022.11.039272

Contents

Abstract. The most important temporal and spectral characteristics of X-ray radiation arising near black holes, neutron stars, and white dwarfs in the presence of matter accreting from the disk that surrounds the compact object are reviewed. It is shown how these characteristics are related to the physical parameters of these systems. A key characteristic of X-ray radiation is photon index Γ, defined as the slope of the emission spectrum in the energy range of 0.5–500 keV. If the compact object of a binary is a black hole, the X-ray radiation features saturation of the photon index (with increasing accretion rate), its value is ranging from 2 to 3. A correlation between Γ and the quasi-periodic oscillation frequency, $\nu_{\rm QPO}$, is revealed in these systems, which can be employed to independently determine the black hole mass using scaling method. The developed model of radiation transfer is now the basis of a scaling method which provides an independent estimate of mass also in the case of a supermassive black hole. The generated X-ray spectrum can be presented in a wide energy range as a combination of thermal, Comptonized, and Gaussian components that describe the emission lines. A model of radiative transfer in the vicinity of black holes and neutron stars can also explain the properties of the X-ray emission when the compact object is a white dwarf. The example of four dwarf novae, U Gem, SS Cyg, VW Hyi, and SS Aur, is used to show that the continuum of the X-ray spectrum of nonmagnetic cataclysmic variables can be described as a result of the Comptonization of soft photons on hot electrons of the accretion cloud that surrounds the white dwarf.

Keywords: accretion, accretion disk, nonthermal radiation mechanism

L G Titarchuk, E V Mikheeva, V N Lukash
Astro Space Centre, Lebedev Physical Institute,
Russian Academy of Sciences,
ul. Profsoyuznaya 84/32, 117997 Moscow, Russian Federation
E-mail: [a] ltitarchuk@asc.rssi.ru, [b] helen@asc.rssi.ru,
[c] lukash@asc.rssi.ru

Received 26 April 2022, revised 6 October 2022
Uspekhi Fizicheskikh Nauk **193** (9) 940 – 970 (2023)
Translated by M Zh Shmatikov

1. Introduction

X-rays are emitted in binaries containing a compact object (black hole (BH), neutron star (NS), or white dwarf (WD)) due to the accretion of matter flowing from the donor star (Fig. 1). Closer examination shows that the main X-ray source is identified with a transition layer: the region between the rotating accretion disk and the surface of the more slowly rotating central object (for example, the light hypersurface for a BH), where the gravitational energy of the falling matter is released.

In standard concepts of the transition layer, the matter accretion rate determines the optical thickness of the layer, whose value, along with the high electron temperature $T_{\rm e}$, leads to the emergence of X-ray radiation (see, for example, [1]). A shock wave is formed at the outer boundary of the transition layer, where the energy of the matter arriving from the disk is released. As a result of the adjustment of the accretion flow to the rotation of the central compact object, a transition layer is formed. This adjustment implies that the

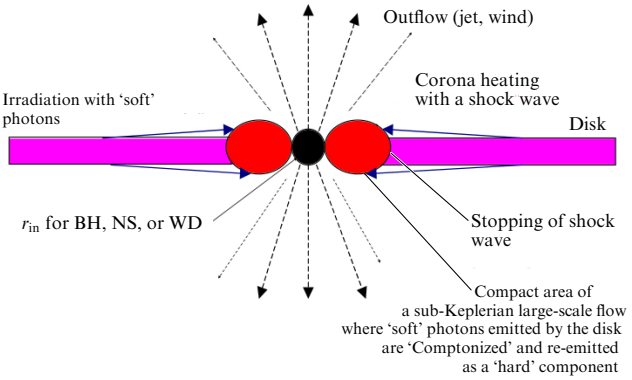

Figure 1. X-ray generation in a binary system. An accretion disk, a hot Compton cloud (transition layer), wind (jet), and a compact object (black hole, neutron star, or white dwarf) are shown.

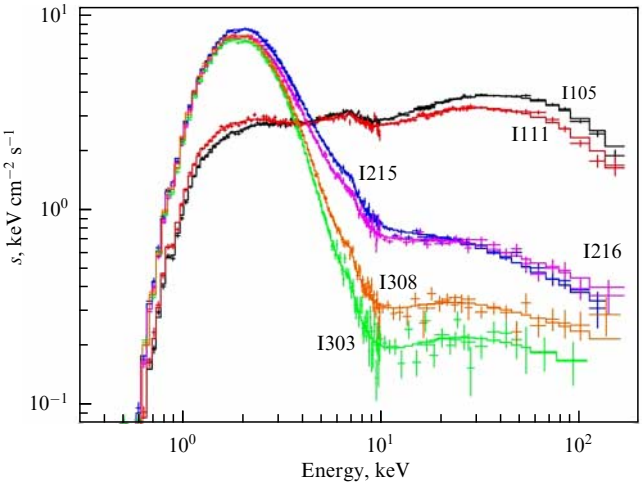

Figure 2. Typical evolution of X-ray energy spectra formed in binary stellar systems with black holes, from a low/hard state to high/soft state using the XTE J1650-500 source as an example. Numbers next to the spectral curves are the timestamps: 1105 and 1111 correspond to the low/hard state, while the rest of the spectra correspond to the high/soft state [10].

angular velocity of the accretion flow at the inner boundary of the transition layer is equal to the rotation velocity of the central object; the derivative of the angular velocity with respect to the radius lies within certain limits; and, at the radius of the junction of the transition layer with the outer Keplerian disk, the angular velocity of the accretion flow should be equal to the Keplerian angular velocity.

The authors of [2] assumed that, at a high accretion rate close to the Eddington value[1] ($\dot{M} \geqslant 10^{18}$ g s^{-1}), the transition layer becomes optically thick and radiates as an absolutely black body with temperature $T \sim 10^5$ K. Respectively, at a low accretion rate ($\dot{M} < 10^{18}$ g s^{-1} or $\dot{m} \ll 1$), i.e., in a state of relative rest, the transition layer has a low density and is optically thin. Since the cooling of the optically thin plasma is less efficient, the temperature of the transition layer becomes higher. In this case, a thermal bremsstrahlung component arises in the spectrum of the binary, which is hard X-ray radiation with a characteristic temperature $T \sim 10^8$ K [3]. Part (up to half) of such radiation should be absorbed by a compact object (NS or WD) and re-emitted in the soft X-ray range with an effective temperature of $T_{\rm eff} \leqslant 10^5 - 10^6$ K (see, for example, [3–5]). The spectra of X-ray systems, in which a BH, NS, or WD is the compact object, are well described by Comptonization models, such as COMPTT [6–8] or COMPTB [9], characterized by a relatively small number of parameters (see a description of models and parameters on the site of the XSPEC public software package[2]).

A number of relations or correlations can be established between the spectral and temporal characteristics of sources where a BH is the compact object. These relations show the evolution of properties during the transition from a hard state to a soft one, when the radiation hardness (in other words, the spectral index α) changes.[3] Figure 2 shows an example of the evolution of X-ray spectra from the hard state (spectra 1105-1111) to the soft state (spectra 1303-1308) in the XTE J1650-500 source, which, apparently, contains a BH.

The X-ray source spectrum $J(E)$ can be represented in the general form as a linear superposition of blackbody radiation from the accretion disk BB(E) and part of this radiation f, convolved with the Comptonization Green's function $G(E, E_0)$ (see [11]):

$$J(E) = C_{\rm N}\left(\frac{\rm BB(\mathit{E})}{1+f} + f\,{\rm BB}\,G\right), \qquad (1)$$

where $C_{\rm N}$ is the normalized flux of soft photons from the disk. It is of importance to emphasize that the shape (1) of the resulting Comptonization spectrum from compact sources is the general one and does not depend on the source type (BH, NS, or WD). The parameters of this model are the color temperature of the blackbody component BB, the spectral index α (or the photon index $\Gamma = \alpha + 1$) of the Comptonization Green's function $G(E, E_0)$, the fraction of soft (outgoing from the disk) photons intercepted by the Compton cloud, f, and the normalized flux $C_{\rm N}$ of photons from the disk, which is proportional to the accretion rate and the mass of the central object.

It should be noted that the described approach does not imply the use of a specific model of disk accretion (for disk accretion models, see review [12] and references therein), which, like any model, has limited application. The spectral model under consideration is based on the fact that the resulting spectrum of an X-ray source is the sum of direct blackbody radiation with a temperature of about 1 keV for galactic compact sources of stellar masses (BH or NS) or a fraction of 1 keV for extragalactic sources and the Comptonized component. In the case of an NS, it also contains an additional blackbody component with a temperature on the order of a fraction of 1 keV, due to the contribution of radiation from the accretion disk. An additional Comptonization component is the convolution of a certain fraction of blackbody radiation with the Comptonization Green's function (see, for example, [11]). Thus, the presented structure of the spectrum is, in a certain sense, a 'theorem' of

[1] The accretion rate $\dot{M}$ corresponds to the value of the dimensionless accretion rate $\dot{m} \equiv \dot{M}/\dot{M}_{\rm Edd} \geqslant 1$, where $\dot{M}_{\rm Edd} = L_{\rm Edd}/(\eta c^2)$, $\eta = 0.1$ is the accretion efficiency, $L_{\rm Edd}$ is the Eddington luminosity, and c is the speed of light.

[2] https://heasarc.gsfc.nasa.gov/xanadu/xspec/.

[3] The degree of radiation hardness implies two close qualitative concepts. The first is the change in the shape of the radiation spectrum (presented, as a rule, in energy units) in the course of evolution when one state of the source successively converts into another. The second, more formalized, concept implies the movement of the source on the 'color–color' or 'soft color–hard color' diagram. This refers to the ratio of intensities in the energy range, for example, (3.5–6 keV)/(2–3.5 keV) ('soft' color) to a value in the range of (9.7–16 keV)/(6–9.7 keV) ('hard' color).

radiation transfer for compact objects. Our review is devoted to the Compton model of X-ray emission from the accretion flow onto compact objects, which has been successfully used for 40 years and is based on the single assumption regarding the blackbody nature of disk photons. Of course, in some cases, this model may fail (for example, when the BH rotates very strongly or the dynamics of the accretion disk is greatly influenced by its magnetic field). A discussion of various disk models is beyond the scope of our review.

The considered structure of the spectral model sets the number of parameters that are determined as a result of its fitting to the observed spectral data. There are only five of these parameters: (1) the color temperature of blackbody radiation, which provides the so-called soft (seed) photons for Comptonization; (2) the spectral index of the Green's function α; (3) the fraction of soft photons f that are Comptonized in a relatively hot Compton cloud; (4) the plasma temperature of the Compton cloud T_e; and (5) the normalization of soft (seed) photons proportional to the accretion rate. The experience of using the Comptonization model (COMPTB in the XSPEC package mentioned above) confirms that spectral X-ray data are excellently approximated by the Comptonization model.

The scaling method developed for X-ray binaries (see [13]) turned out to be very successful also for extragalactic ultraluminous sources (for example, M101 ULX-1) and for supermassive BHs in active galactic nuclei (NGC 4051, 3C 454.3, etc.). This became possible due to the discovery of correlations between the photon index Γ and the accretion rate observed in the nuclei of these galaxies (see [14]). It is worth noting that a characteristic of the correlation of the photon index Γ with ν_L, the lowest frequency of quasi-periodic oscillations (QPOs), is that ν_L is inversely proportional to the BH mass and, thus, for the same Γ, the lowest QPO frequencies will differ according to the relation $\nu_{L,1}/\nu_{L,2} = m_{\mathrm{BH},2}/m_{\mathrm{BH},1}$, where $m_{\mathrm{BH},1}$ and $m_{\mathrm{BH},2}$ are the black hole masses. In turn, in the correlation of Γ with the accretion rate or normalization N, which is proportional to the BH mass, for the same Γ, the values of N for two sources will differ according to the relation $N_1/N_2 = m_{\mathrm{BH},1}/m_{\mathrm{BH},2}$. These relations underlie the scaling method for estimating BH masses.

Using Eqn (1) for the X-ray spectrum, 17 transitions from a hard state to a soft state were analyzed in [13] for eight X-ray binaries containing BHs (observational data were obtained using RXTE[4]). On the other hand, based on the energy balance equation and the diffusion transfer equation for the transition layer in the case of an NS, a formula was derived in [15] for the spectral index α for thermal Comptonization. As a result, it was possible to show that, in this approximation, in the transition layer, there should be a relationship between the electron (plasma) temperature of the corona T_e, the optical thickness τ_0, and the ratio of the energy flux from the disk intercepted by the transition layer, Q_{disk}, and the corona radiation, Q_{cor}. In principle, the spectral index α depends on the electron (plasma) temperature of the corona T_e, and it turns out that $\alpha = f(Q_{\mathrm{disk}}/Q_{\mathrm{cor}}) \sim 1$ at $Q_{\mathrm{disk}}/Q_{\mathrm{cor}} \ll 1$.

This prediction was confirmed by further research. In particular, the authors of [16] analyzed the spectral properties of X-ray radiation from a binary system with an NS, 4U 1728-34, during transitions from low to high luminosity, when the electron temperature T_e of the Compton cloud decreased monotonically from 15 to 2.5 keV. Transition episodes were studied by analyzing data obtained by BeppoSAX[5] and RXTE. It was found that the X-ray spectra of 4U 1728-34 for all spectral states can be modeled by a combination of the thermal (blackbody), Comptonization (which, for definiteness, we will call COMPTB), and Gaussian components. A spectral analysis carried out on the basis of this model showed that the photon index Γ in the analyzed data remains almost constant in the course of all these spectral transitions. The last interesting observation is explained by the dominance of a powerful Comptonization component in this source, which is formed in the transition layer. Consequently, the quasi-constancy of Γ is realized when the energy released in the transition layer is much greater than that of the flux coming into the transition layer from the accretion disk. Moreover, the stability of the photon index established for the spectral evolution of the 4U 1728-34 source has also been confirmed for a number of other binaries with NSs, namely: 4U 1700-37, 4U 1705-44, Sco X-1, GX 340 + 0, 4U 1820-30, and GX 3 + 1. This property of the sources fundamentally differs from that observed for systems with a BH, in which Γ monotonically increases during the spectral transition from a low to a high state and saturates at large values at large accretion rates $\dot{m} > 1$.

Studies have shown (see [17]) that the Comptonization model can also be used to describe the emission continuum of cataclysmic variables, where matter is accreted onto a white dwarf that has a relatively low magnetic field or belongs to the Intermediate Polars[6] (IP) type. Since structural properties of such systems are common with those of low-mass X-ray binaries (LMXBs), i.e., they contain an accretion disk, a transition layer (corona), and a compact object (see Fig. 1), it is logical to assume that, in this case, the same physical processes occur and, consequently, the spectral continuum of cataclysmic variables[7] can be successfully described by Comptonization (scattering 'up') of soft photons on hot electrons of the Compton cloud.

As noted above (see also [18]), the photon index Γ for neutron stars is ~ 2. Study [15] analytically demonstrated that this is the result of the release of the gravitational energy of the accreting matter in the transition layer near the NS surface. A similar effect should also be observed in white dwarfs, where it is necessary to take into account the absorption of X-rays by the WD surface, while X-rays are reflected from the NS surface.

2. Black holes in X-ray systems: temporal and spectral manifestations, interpretation

2.1 Black holes in our Galaxy

Observational manifestations of black holes in the X-ray range, as a rule, can be described in terms of spectral states

[4] Rossi X-ray Timing Explorer is an orbital X-ray observatory. https://heasarc.gsfc.nasa.gov/docs/xte/XTE.html.

[5] Space station for observation in the X-ray range. Beppo is the surname of a famous Italian physicist. SAX is an abbreviation of Italian name Satellite per Astronomia a raggi X (astronomic X-ray satellite) (https://heasarc.gsfc.nasa.gov/docs/sax/sax.html).

[6] IP or intermediate polars are the white dwarfs included in binary systems; their magnetic field is $10^6 - 10^7$ G and the rotation period is less than the orbital period (equal to 1– 100 hours).

[7] A cataclysmic variable is a star exhibiting burst (cataclysmic) and other activity, which is a close binary system consisting of a white dwarf and a companion.

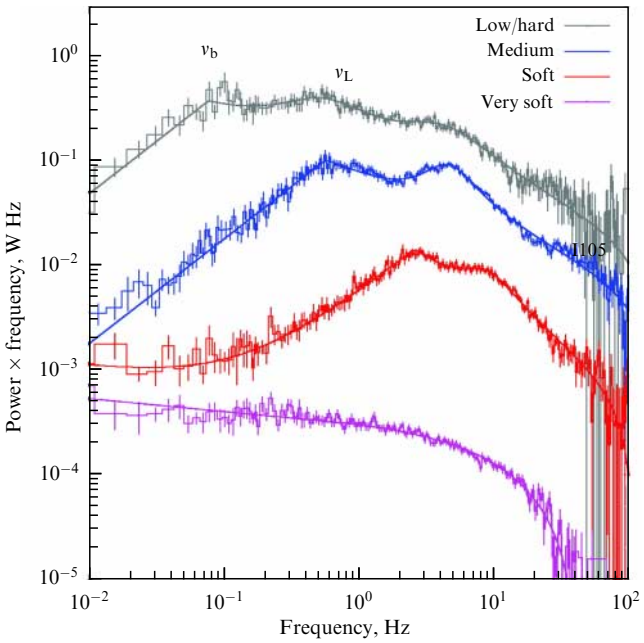

Figure 3. Evolution of the power spectrum of the Cyg X-1 energy spectrum from a low/hard state (at the top of the figure) to a high/soft state (at the bottom of the figure) [22].

(see [19–21]), while the X-ray spectrum itself can be decomposed into three components: blackbody, Comptonization, and several emission lines of iron K_α.

Conventionally, the following states are distinguished in the evolution of emission X-ray sources, which include BHs: quiescent state (QS), low/hard (LHS), intermediate (IS), high/soft (HSS), and, for some sources, very high state (VHS) (see Fig. 2). In describing the sequence, it is logical to start with the quiescent state, which ends when a burst occurs in the source. The source then changes from the quiescent state to a low/hard state, characterized by a lower luminosity in the soft X-ray range and, at the same time, a generally harder spectrum. In terms of spectral components, this implies that the thermal (blackbody) component weakens, while the Comptonization component, which is the result of the Comptonization of soft photons of the accretion disk on hot coronal electrons, is enhanced (see, for example, [10, 11]).

In such a (Comptonization) model, the photon spectrum of X-ray binaries with BHs (see Fig. 2) is due to a thermal component reflecting the manifestation of powerful emission from the accretion disk. A weak power-law component is also present, at a level not exceeding 20% of the total source flux.

Figure 3 shows an example of the evolution of the power spectrum as a function of frequency for a Cyg X-1 source. In the low/hard state, the source exhibits high fractional variability — up to 40% — and the power spectrum is parameterized by a power-law function with a break at frequency ν_b and quasi-periodic oscillations with the lowest frequency ν_L. QPOs, being, in fact, a resonant effect, are not always present in the power spectrum. In the very high/very soft state, the QPOs disappear along with the white-red noise, and the power spectrum of variable X-ray radiation becomes a purely power-law. High/soft state variability is typically less than 5%.

The temporal and spectral properties of accreting BHs are closely related (see a fairly complete list of references in [13]). Both groups are determined by the physical conditions and properties of both the binary system as a whole and its components, of which the BH mass is the most important parameter. The authors of [23] were the first to propose to use relations between the photon index Γ and QPO frequencies to determine BH masses. Subsequently (see [24]), the developed method for determining the masses, called the scaling technique, was also applied to Cyg X-1, as a result of which the mass of the BH in this system was found to be $(8.7 \pm 0.8)\, M_\odot$. This estimate does not disagree with the values found by dynamic methods, but is more accurate. Thus, the scaling method provides an independent estimate of the BH mass.

It is worth noting that study [25] has recently reported the estimated mass of the same BH equal to $(21.2 \pm 2.2)\, M_\odot$, a value which is much higher than that obtained from earlier estimates and ours. The authors of [25] used the following physical parameters derived from fitting for Cyg X-1 (see Table 1 in [25]): inclination i, eccentricity e, orbit periastron argument ω, O-star mass M_1, filling factor of the Roche lobe f_1, effective temperature $T_{\rm eff}$, semi-amplitude of the radial velocity curve K_1 for an O star, shift parameter φ necessary to take into account the ephemeris error, and the ratio of rotation frequency of the O star $\Omega_{\rm rot}$ to its orbital frequency. Thus, the calculations of the BH mass in [25] require nine parameters to be determined from observations. In addition, such model parameters are used as black hole mass $M_{\rm BH}$, O-star radius R_1 (expressed in units of solar radius $R_\odot$), luminosity L (also expressed in units of solar luminosity $L_\odot$), the value of surface gravity g_1 for the O-star, magnitude of the semi-major axis of the orbit a, star orbit a_1, and BH orbit $a_{\rm BH}$. The values of the listed seven parameters were obtained using the above nine fitting parameters for a given value of the orbital period Cyg X-1. We also note that in [25] the dimensionless BH rotation parameter was estimated, $a_* > 0.9985$, implying that the accretion disk comes very close to the gravitational radius $R_{\rm g} = R_{\rm s}/2$, virtually coinciding with it. It might be concluded then that the resulting X-ray spectrum should be described by blackbody radiation from the disk. However, as shown in [24], the resulting spectrum is represented by a strong Comptonization component, in which the photon index Γ evolves from 1.5 to 2.1 (Fig. 4).

The scaling method was also used to estimate the BH mass in ultraluminous X-ray sources GRS 1915 + 105 and XTE J1550-564 [23], M82 X-1 [26], M81 X-9 [27], and NGC 5408 X-1 (see [28] and references therein). Note that some of the listed sources include BHs of intermediate masses lying in the range of $(100-250)M_\odot$.

The method of scaling by correlations Γ with the QPO frequency, combined with scaling by correlation Γ with the accretion rate, was used in [13] to estimate BH masses and distances to galactic sources H 1743-322, GX 339-4, XTE J1550-564, XTE J1650-500, 4U 1543-47, XTE J1859 + 226, and Cyg X-1. Previous estimates of the BH masses, distances to sources, and orbital inclination were used as additional data: microquasar GRO J1655-40 was used as a reference source.

For the analysis, the archived RXTE data from HEASARC[8] were employed, namely, the Proportional Counter Array (PCA) data, from which the power spectra were constructed. Corrections for 'dead' time in the energy and

[8] High Energy Astrophysics Science Archive Research Center, http://heasarc.gsfc.nasa.gov/.

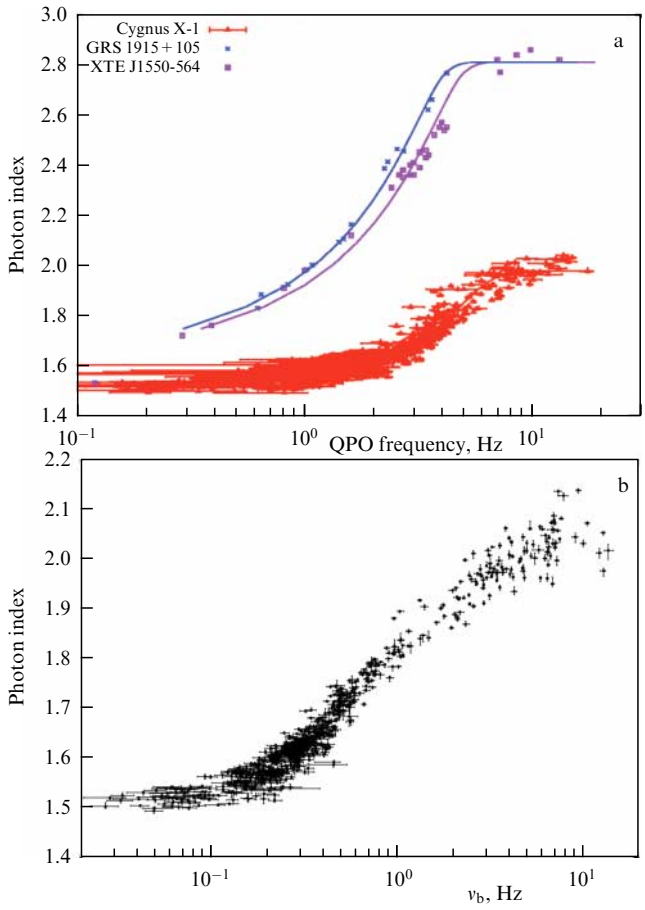

Figure 4. Correlation of the photon index of Comptonization spectrum Γ in the Cyg X-1 source with (a) the QPO frequency and (b) the frequency of the break in the power spectrum ν_b according to data obtained by RXTE. Corresponding correlations are also displayed for GRS 1915+105 and XTE J1550-564 [22].

temporal spectra were made following the recommendations set out in *The RXTE Cook Book* and [29], respectively. Next, the PCA spectra were modeled using the XSPEC software, and each spectrum was considered as the sum of a Bulk Motion Comptonization (BMC) component (see a more detailed description of the model in [30]) and a Gaussian with an energy of ~ 6.5 keV, modeling the emission line of iron. Furthermore, interstellar absorption was added to the model: the absorption of the hydrogen column along the line of sight N_H was taken equal to that given by the HEASARC code (see [31]) for each source with a spectrum cutoff at high energies. The width of the Gaussian was limited to the range of 0.8–1.2 keV. The high-energy cutoff of the component makes it possible to take into account the exponential dip in the spectrum due to the electron recoil effect. Finally, all RXTE/PCA spectra were assigned a systematic error of 1%. Note that the model describes the spectrum outgoing from the source as a convolution of the spectrum of soft blackbody photons characterized by the color temperature T_c, normalized by N_{BMC}, with the Green's function for Comptonization. As usual, the N_{BMC} normalization implies normalizing to the Eddington luminosity of a star with the solar mass and the distance to the source squared:

$$N_{BMC} = \left(\frac{L}{10^{38}\ \text{erg s}^{-1}}\right)\left(\frac{10\ \text{kpc}}{d}\right)^2. \qquad (2)$$

The resulting spectrum is characterized by the parameter $\log A$ associated with the fraction $f \equiv A/(1+A)$ of Comptonized photons in the emission and the spectral index of the Green's function $\alpha \equiv \Gamma - 1$.

There are two main reasons for using the BMC model. The first is that the model can be applied in the general case when photons gain energy not only due to thermal Comptonization but also when Comptonization is dynamic (see [22, 30, 32]). The second reason is that the BMC model is related to the normalization N_{BMC} of seed photons, which in the case of a BH are produced in the accretion disk. The normalization N_{BMC} is proportional to the disk accretion rate, i.e., is directly related to the accretion disk model (see, for example, [33]). The adopted spectral model describes well the overwhelming majority of the data analyzed in [13], i.e., the value $\chi^2_{red} = \chi^2/N_{dof}$, where N_{dof} is the number of degrees of freedom in a given fit, is close to unity, and only for a small fraction ($< 3\%$) of all spectra does the value χ^2_{red} increase to 1.5.

The power spectrum in the low/hard and transient states has the form of limited noise, which can be described by the empirical formula

$$P_X \sim \left[1.0 + \left(\frac{x}{x_\star}\right)^2\right]^{-in},$$

where parameter $x_\star$ is equal to the characteristic frequency of the break in the power spectrum and $2 \times in$ determines the slope of the power spectrum after the break. It should also be noted that a Lorentzian profile was used to fit the QPO.

Processing of the BeppoSAX data revealed saturation of the spectral index with an increase in the accretion rate (see [10]), which can be considered observed evidence of a converging flow for XTE J1650-500 (see details in [34]).

It is important to note that, when the source attains a high/soft state, the white-red noise variability disappears along with the QPO manifestations, and the power spectrum acquires a pure power-law form. The total variability in the high/soft state is on the order of 5% rms. The correlations of the photon index Γ with the QPO frequency and BMC normalization are shown in Figs 5a and 5b during the rise of an X-ray burst in XTE J1550-564 in 1998. Two different tracks of the Γ correlation with the QPO frequency correspond to different saturation levels of the index.

The burst began at MJD 51063 (MJD; Modified Julian Date) and passed via an initial low/hard state that ended at MJD 51069. During this transition, the photon index Γ increased from 1.3 to 2.2, and the QPO frequency increased from 0.3 to 3.3 Hz (this phase is marked in Fig. 5 with black dots). Over the next 10 days, the source exhibited an intermediate state with a strong burst on MJD 51076 (these data are marked with red dots) when the QPO index and frequency reached 2.8 and 14 Hz. After the burst, the source returned to the intermediate state with a photon index of ~ 2.3 and QPO frequency of ~ 3 Hz. Over the next 20 days, a gradual evolution to the high/soft state could be observed, with the photon index slightly increasing to 2.5 and the QPO frequency reaching ~ 5 Hz. Around MJD 51105, the source entered a high/soft state.

Figures 6a, b show the spectral evolution of another X-ray source, GRO J1655-40, presented as a change in the light curve (PCA) and radiation hardness defined as the ratio of fluxes in the energy ranges of 9–20 keV and 4–9 keV. The correlations of the photon index Γ with the QPO frequency,

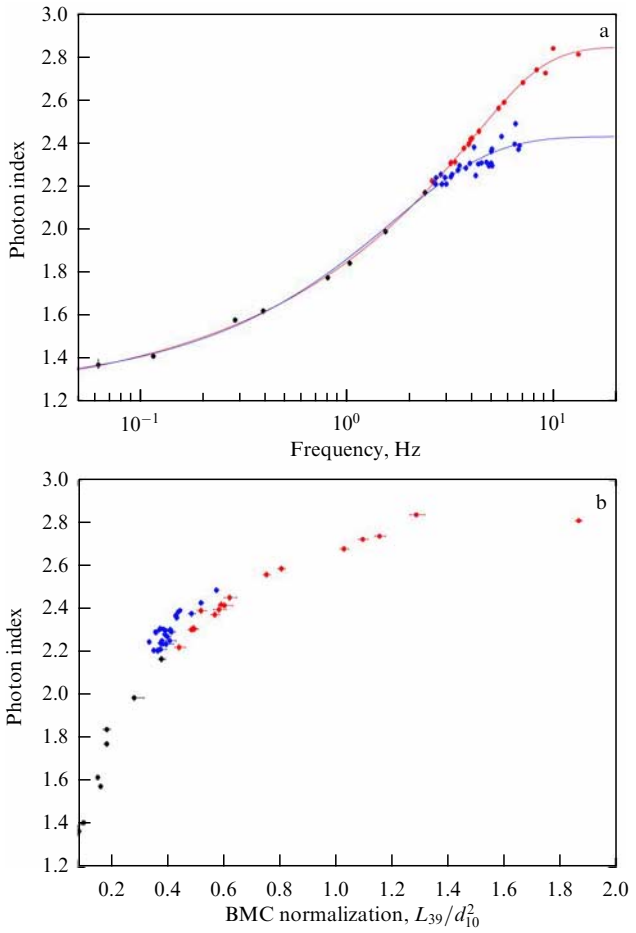

Figure 5. Correlations of photon index Γ with the QPO frequency (a) and BMC normalization (b) during a burst in XTE J1550-564 in 1998. Two different tracks in panel a correspond to two different levels of index saturation [13].

the normalization $N_{\rm BMC}$, and the Comptonized radiation fraction $f \equiv A/(A+1)$ are shown in Figs 6c–e.

Thus, the QPO frequency and BMC normalization correlate with the photon index Γ, while the fraction of Comptonized radiation f and the Γ index usually anticorrelate (Figs 6c–e). In the upper part of the correlations, we observe saturation of Γ, which is best seen in plots of Γ versus normalization (proportional to the accretion rate) rather than in plots of Γ versus QPO frequency. This observation is of importance, because Γ and the spectrum normalization can be determined independently from the spectral state of the source, while QPOs become weak and completely disappear when the source enters the high/soft state.

The saturation of the photon index Γ in the GRO J1655-40, Cyg X-1, and GRS 1915+105 sources was first reported in [24]. Later, the saturation effect was confirmed for Cyg X-1 in the 2001–2002 observations (Fig. 7) (see also Figs 3–6). Moreover, the saturation of the index was found in the XTE J1650-500, GX 339-4, H 1743-322, and 4U 1543-47 sources (Figs 6, 8–10). The saturation of the index with respect to spectrum normalization in XTE J1650-500 was revealed in [10] in analyzing the BeppoSAX data for the 2001 burst. A similar behavior is observed for all transitions from a low/hard state to the high/soft state in XTE J1550-564, H 1743-R03, and J1859-R99 (see [13]).

For the next step, it is of importance that the available Γ–normalization relationships indicate the absence of a hysteresis effect for the Cyg X-1 source. This phenomenon can be associated with a relatively constant rate of wind accretion due to the optical component. Thus, data on the rise and fall of the flux from Cyg X-1 can be used to derive a correlation pattern.

During periods of decay, the source luminosity is lower than during periods of rise, and the variability is suppressed. As a result, spectral and temporal data are associated with decay transitions when the signal-to-noise ratio (S/N) is lower than that observed for rise transitions. The saturation levels of the photon index for the decay phases are close to 2.1. Most likely, this is due to the fact that, at low accretion rates characteristic of decay, the cooling of the X-ray emission region (Comptonization cloud) by photons from the disk is less efficient than at high accretion rates. As a result, the plasma temperature in the Compton cloud $T_{\rm e}$ rises, thereby leading to more efficient Comptonization and a harder spectrum. Such a direct relationship between $T_{\rm e}$ and the hardness of the resulting spectrum was shown in [32] using Monte Carlo simulations. Thus, periods of decay are different from periods of rise, and the index saturates at different levels.

To illustrate all the nuances noted above, we consider the properties of spectral transitions in GX 339-4. This source has five different (rise and decay) transitions, represented by five different tracks (see the third and fourth rows in Fig. 8). The two rise transitions, GX339-R02 and GX339-R07, involve higher fluxes than the two decay transitions, GX339-D03 and GX339-D07. These rise transitions also exhibited steeper photon index–QPO frequency (photon index–normalization) relations with higher saturation levels. On the other hand, GX 339-4, in transiting from the hard to soft state, is like a decay track with index saturation at a level of 2.15. The decay during the 2004 burst was very fast and did not show sufficient activity in the QPO.

Apparently, conditions in the accretion flow change between episodes. During the transition and high/soft states, the source likely entered a phase of a large increase in the accretion flow. This intense flow provided strong cooling, which manifested itself in an increase in the photon index. Figures 9 and 10 show the resulting complex correlations in sources H 1743-322 and 4U 1543-47. It is worth noting the significant saturation of the photon index Γ with respect to the BMC normalization at a level of 3 in the case of H 1743-322. According to [32, 35], this saturation level corresponds to the plasma temperature of the converging flow $T_{\rm e} \sim 5$ keV and below. At the same time, in 4U 1543-47, we see a strong saturation of the photon index at a level of 2.1, and the BMC normalization changes by a factor of four. According to [32, 35], such a saturation level for 4U 1543-47 corresponds to the temperature of the converging flow $T_{\rm e} \sim 10-15$ keV. As for the correlations of Γ with the QPO frequency, the saturation of Γ is barely noticeable for these two sources.

2.2 Scaling method and parameterization of correlated samples

One of the goals of studying BHs is the use of X-ray observations to obtain the fundamental characteristics of these sources.

First of all, X-ray observations should be used to test the theoretical conclusion that the lowest of the QPO frequencies is inversely proportional to the black hole mass $m_{\rm BH} \equiv M_{\rm BH}/M_\odot$ (see [1, 23]). This dependence of the QPO frequency on the mass $m_{\rm BH}$ is a simple consequence of the fact that all characteristic dynamic time scales in a flow

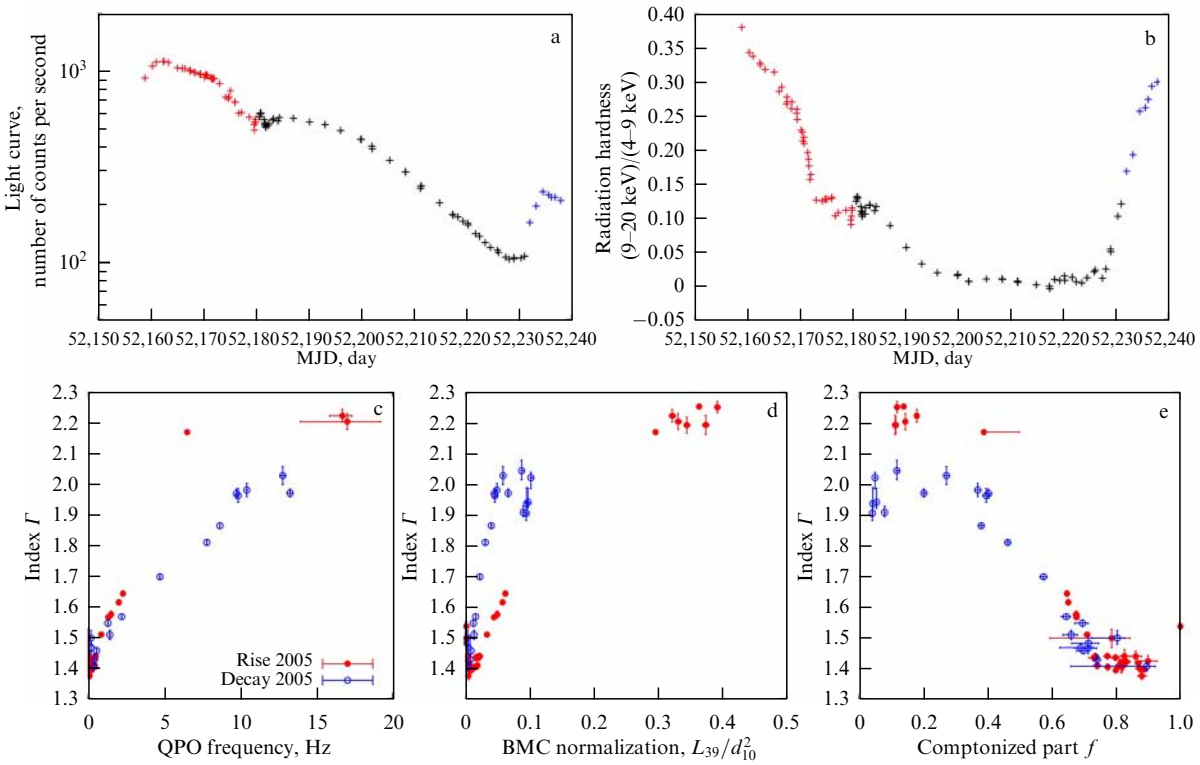

Figure 6. Light curve (a) and variation in radiation hardness (b) for the burst of the GRO J1655-40 source detected in 2005. Photon index as a function of the QPO frequency (c), normalization $N_{\rm BMC}$ (d), and the fraction of Comptonized radiation (e). Red and blue colors indicate transitions of rise and decay, respectively [13].

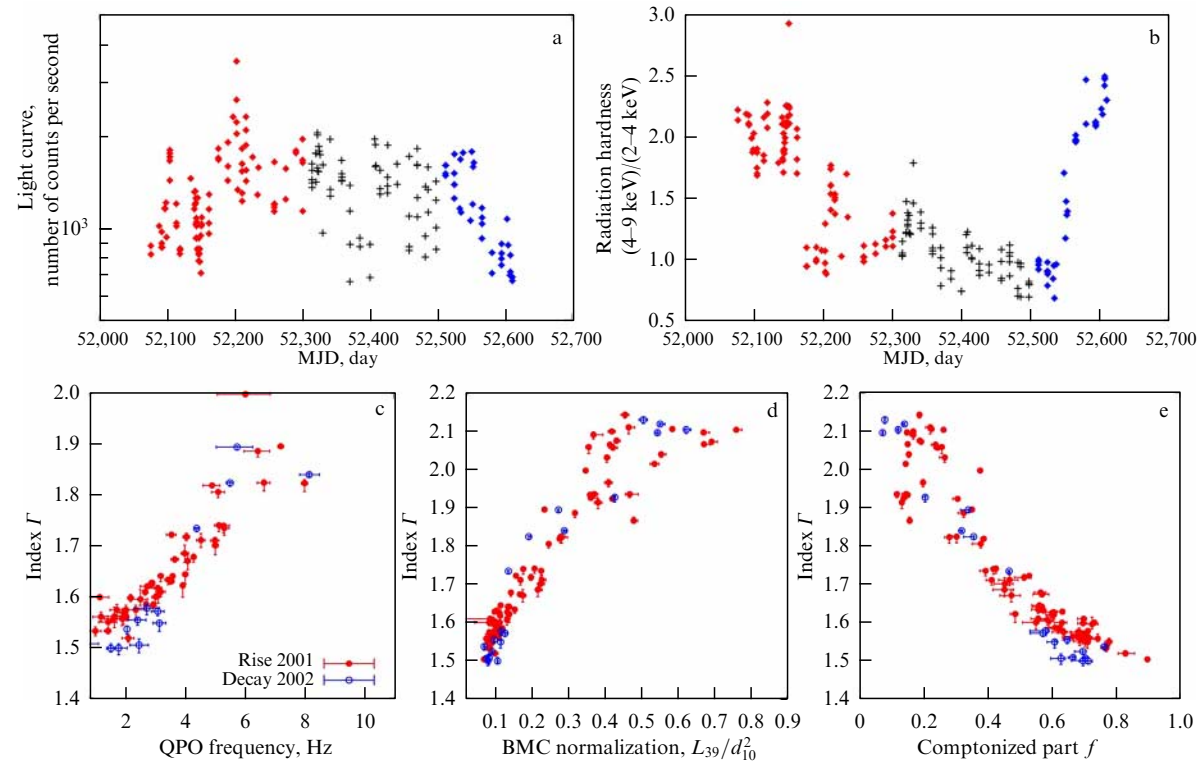

Figure 7. Light curves (a) and radiation hardness (b) for Cyg X-1 in 2001–2002. Red symbols correspond to the transition from a high/soft state to a low/hard state, and blue symbols correspond to the reverse transition. Data from observations during the transition state are shown in black. Photon index as a function of the QPO frequency (c), BMC normalization (d), and Comptonization fraction (e) [13].

accreting onto a compact source depend on the mass of the object (see, for example, [33] and below in this review). Thus, the QPO frequencies, being inversely proportional to these time scales, are inversely proportional to the BH mass (see also [13]). This assumption has now been confirmed by observations.

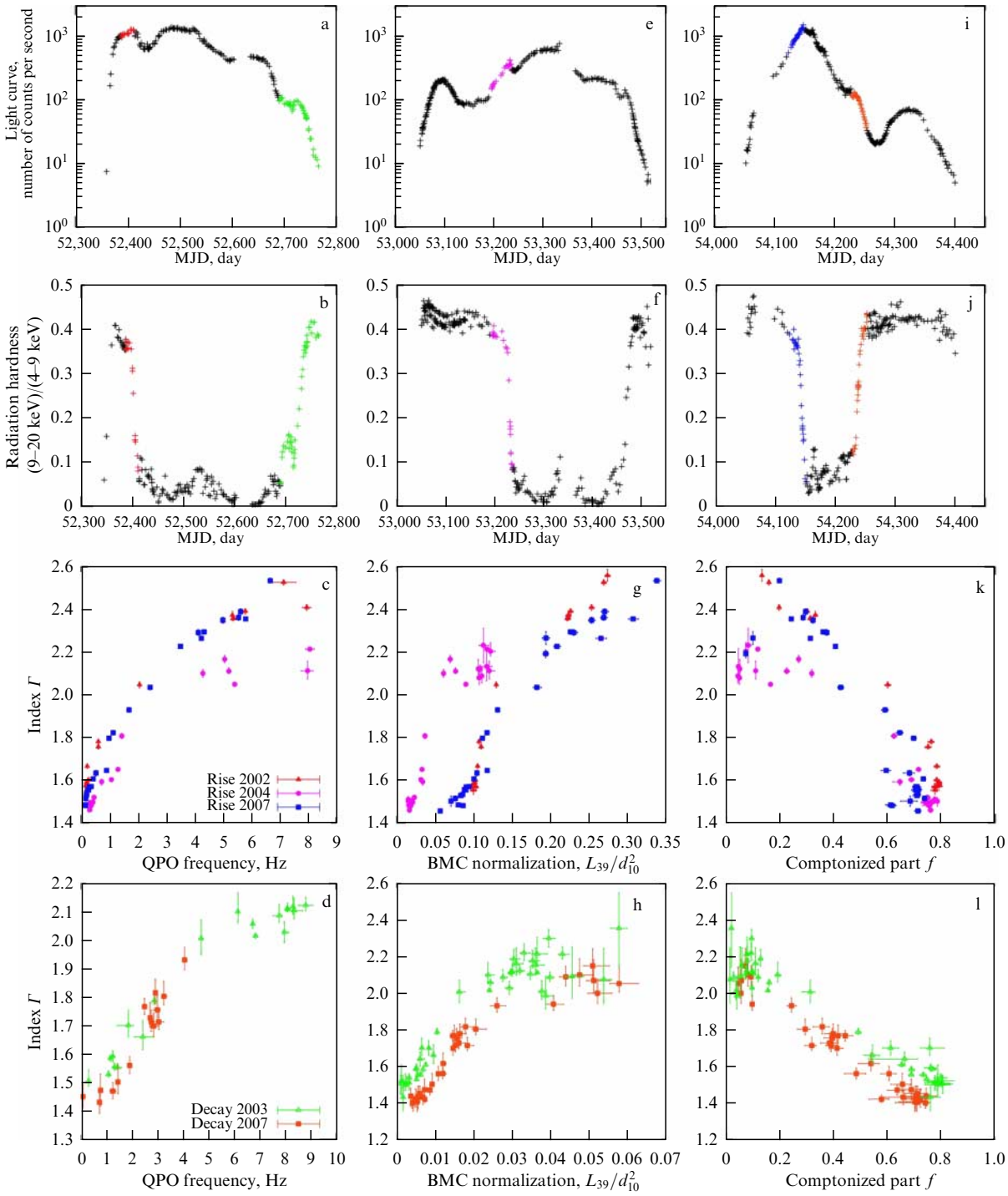

Figure 8. Observational data for three GX 339-4 bursts detected in 2002 (a–d), 2004 (e–h), and 2007 (i–l). Light curves (a, e, i), variations in the radiation hardness (b, f, j), correlations of the photon index and QPO frequency (c, d), BMC normalization (g, h), and Comptonized fraction (k, l) for spectral transitions in GX 339-4 [13].

Thus, we can formulate the *first scaling law* (which was applied to determine the BH mass) using the scaling factors:

$$s_\nu = \frac{\nu_\mathrm{r}}{\nu_\mathrm{t}} = \frac{M_\mathrm{t}}{M_\mathrm{r}}\,, \tag{3}$$

where the subscripts r and t denote the reference and target source, respectively.

The *second scaling law*, which can be used as a basis for estimating the mass of and distance to a BH, sets the ratio of the fluxes F coming to the observer:

$$\frac{F_\mathrm{r}}{F_\mathrm{t}} = \frac{L_\mathrm{r}}{L_\mathrm{t}}\,\frac{d_\mathrm{t}^2}{d_\mathrm{r}^2}\,, \tag{4}$$

where L is the isotropic luminosity of the source and d is the distance to it. The source luminosity can be represented as

$$L = \frac{GM_\mathrm{BH}\dot{M}}{R_*} = \eta(r_*)\dot{m}L_\mathrm{Edd}\,, \tag{5}$$

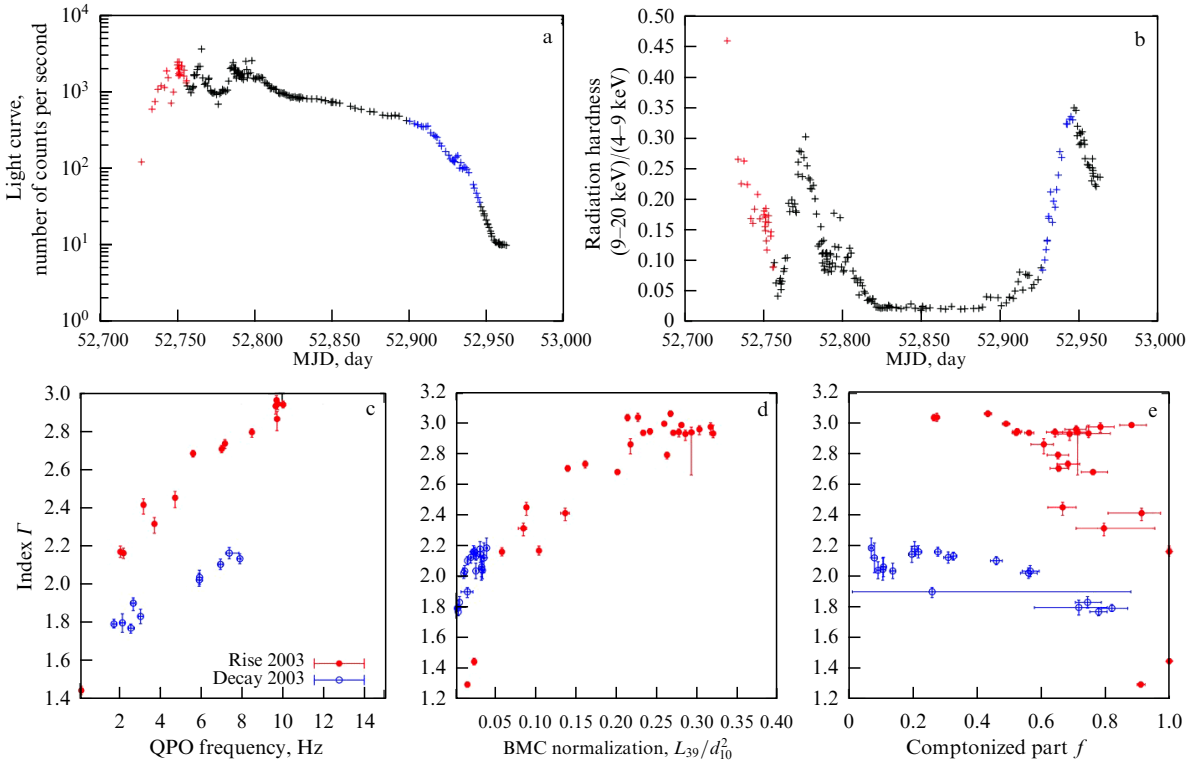

Figure 9. Light curve (a) and radiation hardness (b) for periods of rise and decay in the N 1743-322 source for 2003. Photon index as a function of the QPO frequency (c), BMC normalization (d), and Comptonized fraction (e) for rise and fall transitions [13].

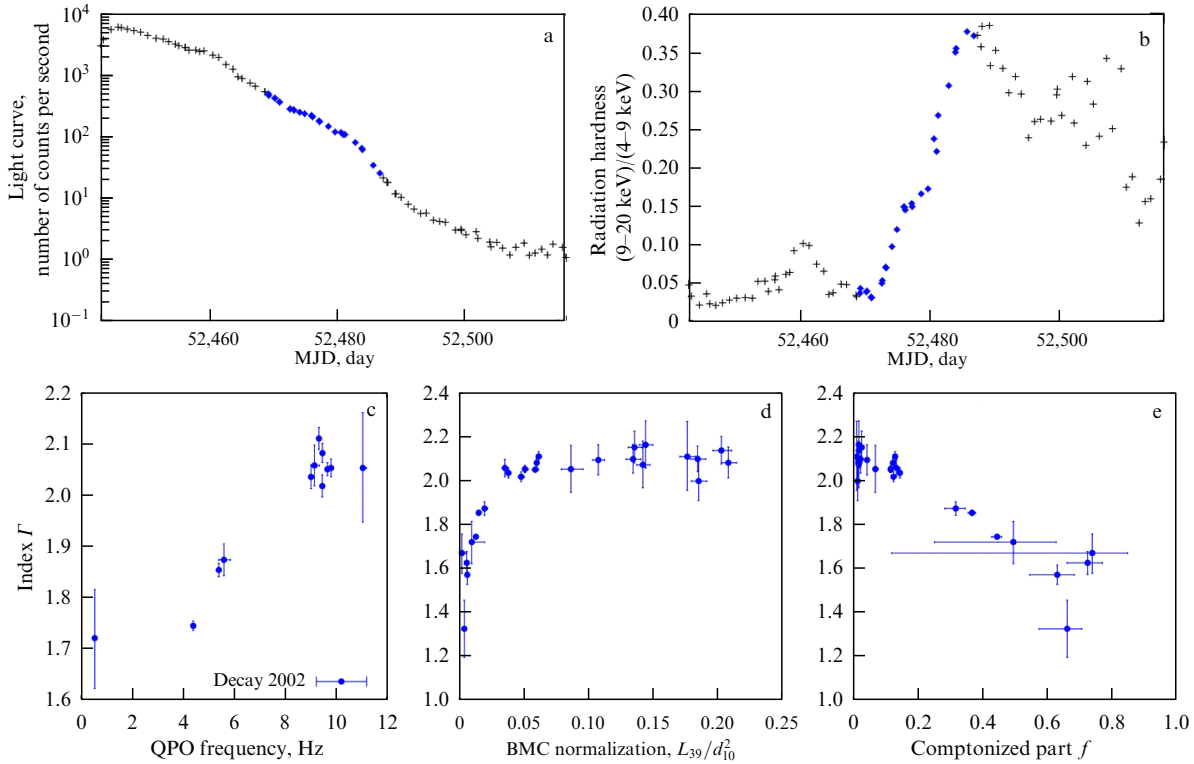

Figure 10. Light curve (a) and hardness (b) for the burst of the 4U 1543-47 source detected in 2002. Photon index as a function of QPO (c), BMC normalization (d) and Comptonized fraction (e) for the decay period [13].

where $R_* = r_* R_S$ is the radius of the disk on which the main energy releases (effective radius), $R_S = 2GM_{BH}/c^2$ is the Schwarzschild radius, the efficiency of gravitational energy release $\eta = 1/2r_*, \dot{m} = \dot{M}/\dot{M}_{crit}$ is the dimensionless accretion rate, and L_{Edd} is the Eddington luminosity.

On the other hand,

$$L_{Edd} = \frac{4\pi G M_{BH} m_p c}{\sigma_T}, \qquad (6)$$

i.e., $L_{\rm Edd} \propto M_{\rm BH}$ and, thus, using Eqns (5) and (6), we obtain

$$L \propto \eta(r_*)\,\dot{m}\,M_{\rm BH}\,. \tag{7}$$

Assuming that $\dot{m}$ and η are the same for sources that are in the same spectral states, we find $L_{\rm r}/L_{\rm t} = M_{\rm r}/M_{\rm t} = 1/s_v$ (the BH subscript is omitted).

The ratio of normalizations of the intensities of the seed photons of the disk for the reference and target sources in the same spectral state can be represented as

$$s_N = \frac{N_{\rm r}}{N_{\rm t}} = \frac{L_{\rm r} d_{\rm r}^2}{L_{\rm t} d_{\rm r}^2}\, f_{\rm G}\,, \tag{8}$$

where $f_{\rm G}$ is a geometric factor that takes into account the difference in angles of viewing of the inner part of the disk, which emits soft photons entering the Compton cloud. Therefore, when the radiation comes directly from the disk, $f_{\rm G} = (\cos\theta)_{\rm r}/(\cos\theta)_{\rm t}$, where θ is the inclination angle of the inner part of the disk. Note that the expression for $f_{\rm G}$ may be not very accurate, since the geometry of the inner disk and corona may differ from that of the disk-sphere. Despite this ambiguity in identifying $f_{\rm G}$, the last formula can be used by setting $\theta \sim i$ in it if the information on the system inclinations is unknown. Now, it is possible to derive the final formulas of the analysis using the scaling method. If s_v and s_N have been measured, the mass of and distance to the source under investigation ($M_{\rm t}$ and $d_{\rm t}$) can be calculated as

$$M_{\rm t} = s_v\, M_{\rm r}\,, \tag{9}$$

$$d_{\rm t} = d_{\rm r}\left(\frac{s_v s_N}{f_{\rm G}}\right)^{1/2}. \tag{10}$$

In using Eqns (9) and (10), the problem of determining the mass of and distance to the source under study is reduced to finding the scaling factors s_v and s_N. The corresponding technique was applied in [24]. For transition episodes, the correlation pattern is parameterized by the expression

$$f(x) = A - BD\ln\left[\exp\left(\frac{1-(x/x_{\rm tr})^{\beta}}{D}\right)+1\right], \tag{11}$$

where x is either the QPO frequency ν or the $N_{\rm BMC}$ value. By approximating the corresponding correlation with this function, the values of the constants A, B, D, $x_{\rm tr}$, and β can be found. If $x \gg x_{\rm tr}$, $f(x) \to A$; thus, A has the meaning of the photon index at the saturation level, and β is a power index at $x < x_{\rm tr}$, $x_{\rm tr}$ being the frequency of the onset of the constant index Γ (or the normalization value $N_{\rm BMC}$). The D parameter determines how rapidly the transition occurs. It can be scaled to the sample under study using the $x \to s\,x$ transformation. The use of an analytic function to parameterize correlations makes it possible to avoid theoretical modeling of the relationship between the photon index and the QPO frequency based on some physical model. This approach makes the scaling procedure model-independent.

2.3 Black hole mass and determination of the distance to X-ray binaries

The galactic microquasar GRO J1655-40 is a well-known X-ray binary black hole whose mass and distance have been measured the most accurately of any known stellar-mass black hole. Therefore, it is logical to use the GRO J1655-40 source as a reference for scaling. The orbital inclination angle is known for this source, due to which the determination of the distance is more reliable. However, not all sources analyzed here have transitions directly scalable to GRO J1655-40 data. Such transitions are only available for GX 339-4 and 4U 1543-47, since their photon index saturation levels are the same.

Having estimated the mass of and distance to GX 339-4 BH, we can use this source as a reference for the analysis of XTE J1550-564 and XTE J1650-500. Note that this scaling between GX 339-4 and XTE J1650-500 is possible for both rise and decay phase data. In this case, XTE J1550-564 can be used as a reference for data scaling for H 1743-322 and XTE J1859-226 (see [13]). Finally, using GRO J1655-40 and 4U 1543-47 as references, the BH mass and the distance to Cyg X-1 can be estimated. All obtained estimates of the BH masses, summarized in the table, are illustrated in Fig. 11.

It should be noted that the scaling based on the use of Eqn (8) contains an uncertainty factor $f_{\rm G}$. To eliminate this uncertainty, the observed correlation of the photon index Γ with the QPO frequency can be used (see Fig. 11).

The very existence of the correlation was predicted in the late 1990s in [1], where the authors defined the transition layer as a region located between the boundary of a sub-Keplerian disk with an internal radius $R_{\rm in} = bR_{\rm S}$ ($R_{\rm S}$ is the Schwarzschild radius and b is numerical factor ~ 3) and the first Keplerian orbit (see also [23]).

Numerical calculations have shown that the value of the dimensionless outer radius $r_{\rm out} \equiv R_{\rm out}/R_{\rm in}$ strongly depends on the Reynolds number γ associated with turbulent viscosity (analysis of observational data shows that the value of γ varies in the range of 2–3) when the rotational speed of the central compact object ω_0 is less than the Keplerian frequency $\omega_{\rm K}$ at the outer radius of the transition layer. The fact that $r_{\rm out}$ is a function of the parameter γ implies that the dimensionless thickness of the transition layer (Compton cloud)

Table. Masses of and distances to black holes.*

Name	$M_{\rm dyn}, M_\odot$	i, deg.	$d_{\rm lit}$, kpc	$M_i, M_\odot$	$M_{\rm scal}, M_\odot$	$d_{\rm scal}$, kpc	References
GRO J1655-40	6.3 ± 0.3	70 ± 1	3.2 ± 0.2				[36, 37]
GX 339-4	> 6	—	7.5 ± 1.6	9.0 ± 3.8	12.3 ± 1.4	5.75 ± 0.8	[38, 39]
4U 1543-47	9.4 ± 1.0	20.7 ± 1.5	7.5 ± 1.0	14.8 ± 1.6	9.4 ± 1.4	9.4 ± 1.8	[40, 41]
XTE J1550-564	9.5 ± 1.1	72 ± 5	$\sim 2.5, \sim 6$	9.4 ± 2.1	10.7 ± 1.5	3.3 ± 0.5	[42–44]
XTE J1650-500	$2.7-7.3$	> 50	2.6 ± 0.7	10.6 ± 4.0	9.7 ± 1.6	3.3 ± 0.7	[45, 46]
H 1743-322	~ 11	~ 70	~ 10	—	13.3 ± 3.2	9.1 ± 1.5	[47]
XTE J1859-226	$7.6-12.0$	—	11	12.3 ± 1.7	7.7 ± 1.3	4.2 ± 0.5	[48, 49]
Cyg X-1	$6.8-13.3$	35 ± 5	2.5 ± 0.3	—	7.9 ± 1.0	2.2 ± 0.3	[50, 51]

* $M_{\rm dyn}$ — dynamically determined BH mass, i — inclination of the system, $d_{\rm lit}$ — distance to the source reported in publications, $M_i = M\cos i$.

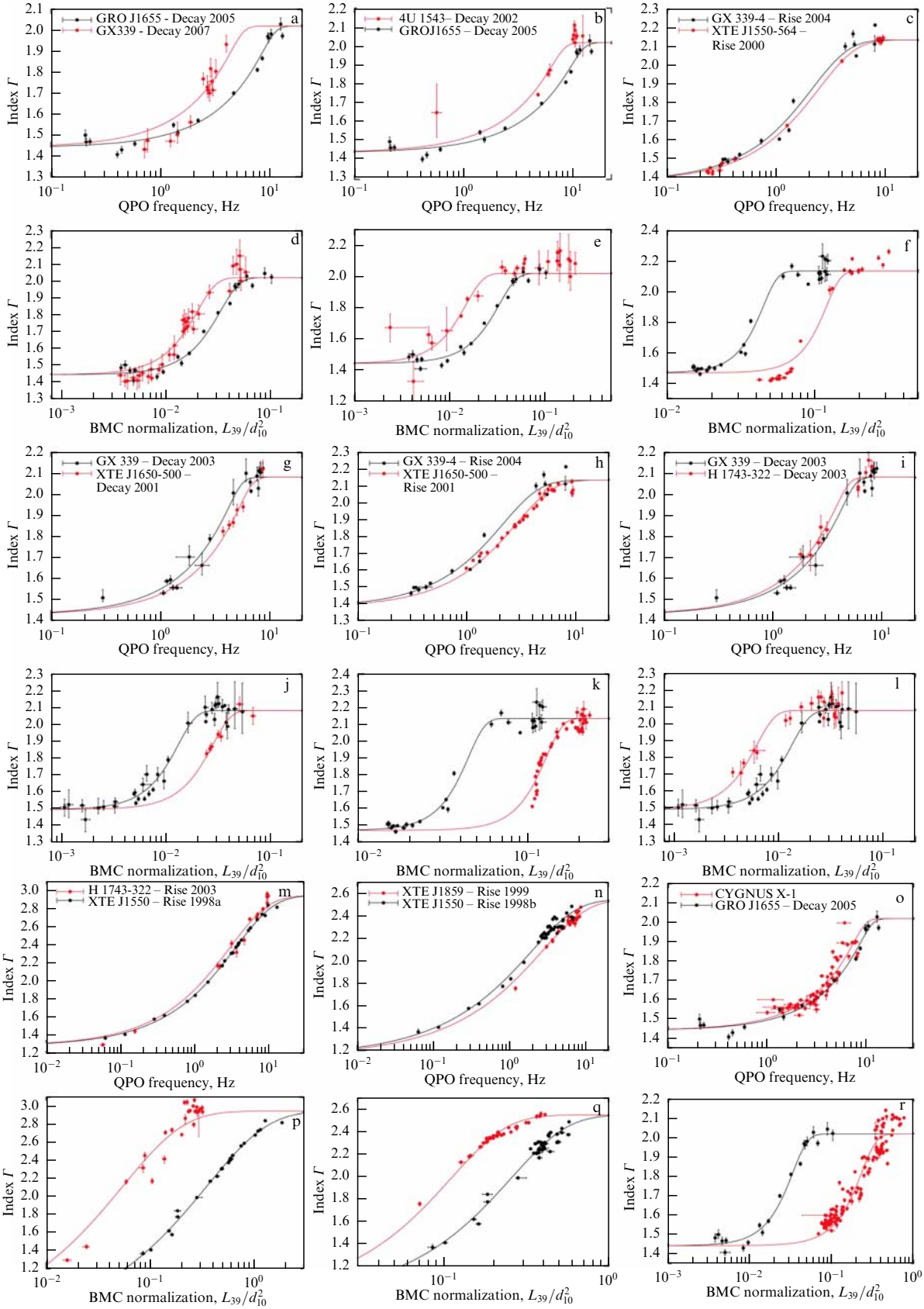

Figure 11. Correlation photon index–QPO frequency and photon index–$N_{\rm BMC}$ normalization for black holes. Studied transition between spectral states is shown in red, and the reference transition is shown in black [13].

$l_{\rm CC} \equiv (R_{\rm out} - R_{\rm in})/R_{\rm in} = r_{\rm out} - 1$ is also a function of γ. In particular, assuming γ to be the parameter that determines the spectral state, we inevitably come to the conclusion that $l_{\rm CC}$ remains constant for a fixed spectral state of an X-ray source

with a black hole, even if the BH masses differ by several orders of magnitude .

Thus, the size of the transition layer (Compton cloud) $L_{\rm CC} = b\,R_{\rm S} l_{\rm CC}(\gamma) = 9\,l_{\rm CC}(\gamma) m$ [km] is proportional to the BH mass $m = M/M_{\odot}$ for the selected spectral state (or γ). Moreover, as shown in [1], the dimensionless extension of the transition layer $l_{\rm CC} = L_{\rm CC}/(bR_{\rm S})$ anticorrelates with the spectral index. The authors of [23] identified the QPO frequency ν_L as that of the normal mode of oscillations of the Compton cloud, which yields, since the QPO frequency is proportional to the ratio of the perturbation propagation velocity in the transition layer to its size, a QPO frequency inversely proportional to the BH mass. In other words, the magnetosonic speed [9] $V_{\rm MA}$ essentially depends on the spectral state. Since the QPO frequency ν_L can be expressed as the ratio of $V_{\rm MA}$ to the size of the Compton cloud $L_{\rm CC}$,

$$\nu_L \propto \frac{V_{\rm MA}(\gamma)}{L_{\rm CC}(\gamma, m)} \approx \frac{V_{\rm MA}(\gamma)}{9 m l_{\rm CC}(\gamma)}\,, \tag{12}$$

the following conclusions can be drawn. First, ν_L should correlate with the spectral state, and second, for a given spectral state, ν_L is inversely proportional to the BH mass. Thus, if the correlation between the index and the QPO frequency persists during the spectral transition and has a shape similar to the correlation shape for another source, the mass ratio of the considered BHs can be determined by shifting the correlation along the $\log \nu_L$ axis relative to each other (see the fine details of applying the scaling technique in [13]). A detailed analysis of the spectral and temporal properties of X-rays radiated from Cyg X-1, which was carried out in [53], confirmed that the QPO frequency ν_L indeed correlates with the Reynolds number γ and the photon index Γ.

The spectral index $\alpha \equiv \Gamma - 1$ characterizes the efficiency of Comptonization, defined as the product of the average relative change in photon energy in one scattering η and the average number of scatterings $N_{\rm sc}$ in the Compton cloud.

In [23], the Monte Carlo simulation of Comptonization processes and directed plasma motion under the action of gravity was used to show that, as the accretion rate increases, Γ first increases and then saturates. Thus, taking into account the existence of correlations of ν_L and Γ with $\dot{M}$, we can conclude that the QPO frequency ν_L should also correlate with the photon index Γ.

The observational data for GX 399-4 and 4U 1543-47 can be scaled with respect to the data for the GRO J1655 source (see [13]), which makes it possible to obtain black hole masses for GX 339-4 and 4U 1543-47 (see Fig. 11). Other transitions for the decay period (GX 339-D03, XTE J1650-D01, and H J1743-D03) feature slightly higher saturation levels of about 2.1, and therefore represent a different sample for scaling.

The GX 339-4 source was also used as a reference source for determining the mass of and distance to a BH which is part of the XTE J1650-500 (Fig. 11g) and H 1743-322 (Fig. 11i) sources. The resulting parameters of the black hole were then used to measure the BH mass of and the distance to XTE J1550-564 (Fig. 11c). The BH mass obtained by the scaling method is in excellent agreement with the value found on the basis of the dynamic characteristics (see the table). Also, transitions GX 339-R04 and XTE J1650-R01 (Fig. 11h) were used as references to provide a double check by scaling the decay data (Fig. 11g) for the same sources. The results obtained by these three independent scaling procedures are in very good agreement.

[9] The magnetosonic velocity arises due to the presence of a magnetic field in the disk, from which the magnetic field penetrates into the transition layer. The influence of the magnetosonic velocity is described in more detail in [52].

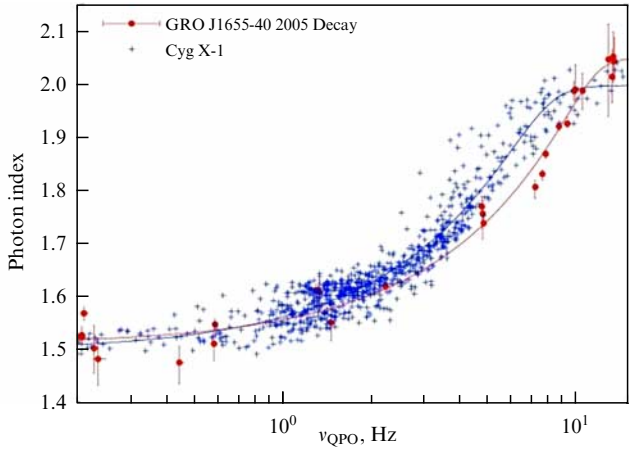

Figure 12. Black hole mass in Cyg X-1 estimated by the method of scaling the $\Gamma - \nu_{\rm QPO}$ correlation [24].

Finally, data from XTE J1550-564 (J1550-R98) were used for scaling in the case of H 1743-322 (1743-R03) (Fig. 11m) and XTE J1859-226 (J1859-R99) (Fig. 11n). As emphasized earlier, during the 1998 burst, two correlation tracks were obtained for the XTE J1550-564 source with different saturation levels of the photon index. The initial low/hard state was combined with a subsequent transition phase from the intermediate state to the high/soft state, similar to the transition in H 1743-322 observed during the 2003 rise (H 1743-R03). Therefore, it was this subset of the XTE J1550 (J1550-R98a) observational data that was used to scale the H 1743-R03 data. The phase of the exit from the intermediate state to the high/soft state of the J1550-R98 source is scaled from J1859-R99 (Fig. 11n). It should also be noted that the XTE J1550-R98, XTE J1859-R99, and H 1743-R03 bursts are similar, not only in the form of the correlations between the photon index and QPO frequency and the photon index and the BMC normalization, but also in the form of the correlation between the photon index and the fraction of Comptonization $(\Gamma - f)$, presented in Fig. 9 using the example of source H 1743-322.

Figures 11o and 12 present the scaling between observational data for GRO J1655 and Cyg X-1. Figure 13 shows the correlation between the Γ index and the QPO frequency for GRS 1915+105 and GRO J1655-40 during the 2005 outburst. The BH mass estimates obtained for Cyg X-1 and GRS 1915+105 are given in the table.

Thus, it is possible to derive a sequence of scaling operations that make it possible to obtain masses of and distances to BHs for a number of X-ray sources in the Galaxy, and in some cases to double check these estimates. The table presents the results for BH masses and distances obtained using the scaling method, together with independent estimates of masses, distances, and orbital inclinations found in the literature. For the sources for which independent estimates can be made using two different data samples, the results of the best fit obtained as the average between individual measurements are presented, and the error range

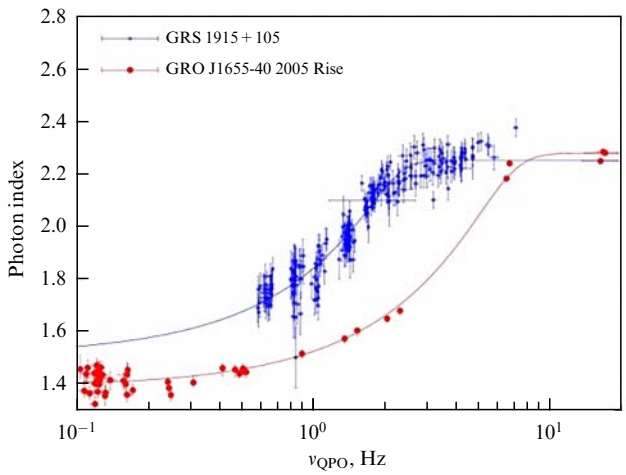

Figure 13. Correlation of photon index Γ with the lower frequency of quasi-periodic oscillations ν_{QPO}. Determination of the black hole mass in the source GRS 1915+105 by the scaling method [24].

was determined from the sum of the error ranges obtained by individual scaling procedures.

2.4 Physical scenario for the evolution of spectral and temporal properties during spectral transitions

The process of accretion onto black holes is far from fully understood. The theoretical models developed to date often deal with limited aspects of the broad observational picture. For example, there are several QPO models (see [20]), most of which only concern the observational manifestations of QPO, while their connection with the spectral properties of radiation and transitions between states are not taken into account. In the concept of the transition layer (Compton cloud), finally, several main observational aspects of accreting BHs are naturally explained, due to which this concept is a strong candidate for the role of the underlying theory of accretion onto compact objects.

The starting point in the development of the transition state concept is the idea of the necessary deviation of the rotation profile from the Keplerian one in the innermost part of the accretion disk. Indeed, the boundary condition near a compact object without a significant magnetosphere is that its rotation is much slower than the Keplerian one. This problem was first raised in [1], where it was shown that the adjustment of the Keplerian rotation in the accretion disk to the sub-Keplerian rotation of the central object inevitably leads to the formation of an internal hot Compton cloud.

2.5 Saturation of the spectral index with respect to the accretion rate as observational evidence of a converging flow into a black hole

As emphasized, positive correlations between the photon index Γ and the QPO frequency should be observed when the corona is cooled by a photon flux coming from the disk [1, 23]. Since the temperature of the transition layer decreases during the transition to the soft state, the effect of dynamic Comptonization becomes dominant in the formation of a hard tail in the final spectral state, i.e., in the high/soft state (see [32, 34]).

As shown in Figs 2, 5–11, index saturation is found in correlations between the photon index and normalization for most sources analyzed, and saturation of the index is sometimes seen in index–QPO frequency correlations. More specifically, saturation of the index was found for the X-ray sources GRO J1655, GX 339, XTE J1550, XTE J1650, H 1743, 4U 1543, and Cyg X-1. The saturation level of the index can vary from one source to another, and even for the same source it can be different for different spectral transitions. For example, GRO J1655-40 exhibits different saturation levels $\Gamma_{sat} \sim 2.3$ and 2.05 during the rise and decline of the 2005 burst (see [24]).

The effect of index saturation with respect to the accretion rate (and the optical depth of the converging flow, τ) was predicted in [34] as a result of the analytical solution of the relativistic kinetic equation (RKE) in the case of a Schwarzschild black hole for a cold plasma, when $kT_e < 1$ keV. Subsequently, this result was reproduced in Monte Carlo simulations (see [32]). Note that the RKE solution was obtained by the method of characteristics, which, in fact, are the trajectories of photons propagating in the gravitational field of a Schwarzschild BH:

$$\frac{x(1-\mu^2)^{1/2}}{(1-x^{-1})^{1/2}} = \frac{x_0(1-\mu_0^2)^{1/2}}{(1-x_0^{-1})^{1/2}} = p\,, \tag{13}$$

where $x = r/r_s$ is the dimensionless radial coordinate, $\mu = \cos\theta$, θ is the angle between the radius vector $\mathbf{r}$ and the line tangent to the photon trajectory, and p is the impact parameter at infinity. For the planar geometry, these characteristics degenerate into straight lines:

$$x(1-\mu^2)^{1/2} = p\,. \tag{14}$$

The saturation of the photon index reflects the fall of plasma into the black hole, since the spectral index $\alpha \equiv \Gamma - 1$ is a quantity inversely proportional to the Comptonization parameter Y, which in turn saturates with an increase in the optical depth τ of the convergent flow or the dimensionless accretion rate $\dot{m}$. Indeed, Y is the product of the average photon energy change in one scattering η and the average number of effective scatterings N_{sc}, i.e., $Y = \eta N_{sc}$.

The preferred direction of propagation for Comptonized photons is along the flow converging on the BH, i.e., along the radius. The fractional change in photon energy is defined as

$$\frac{\Delta E}{E} = \frac{1-\mu_1 V_R/c}{1-\mu_2 V_R/c}\,,$$

where μ_1 and μ_2 are the cosines of the angles between the electron velocities for the directions $\mathbf{n} = \mathbf{V_R}/V_R$ of the incoming and scattered photons. N_{sc} can be estimated as the ratio of the characteristic size of the converging flow along the radius L and the mean free path l: $N_{sc} \propto L/l = \tau$, taking into account that $\Delta E/E$ reaches a maximum $\mu_2 = 1$ for given μ_1 and V_R. On the other hand, the efficiency of one scattering for a converging flow is $\eta \propto 1/\tau$ for $\tau \gg 1$ (see [54]). Thus, the Comptonization parameter Y and the spectral index $\alpha \approx Y^{-1}$ saturate, becoming constants when the optical depth (or accretion rate) of the converging flow increases.

The value of the saturation index is determined by the plasma temperature during the spectral transition (see [32]). On the other hand (see [1]), the plasma temperature strongly depends on the accretion rate in the converging flow $\dot{M}_{bm}$ and its illumination (by the photon flux) by the disk F_{disk}. For large $\dot{M}_{bm}$ and F_{disk}, the plasma temperature is low, on the order of 5 keV. The index saturation level decreases as the plasma temperature in the converging flow increases (see

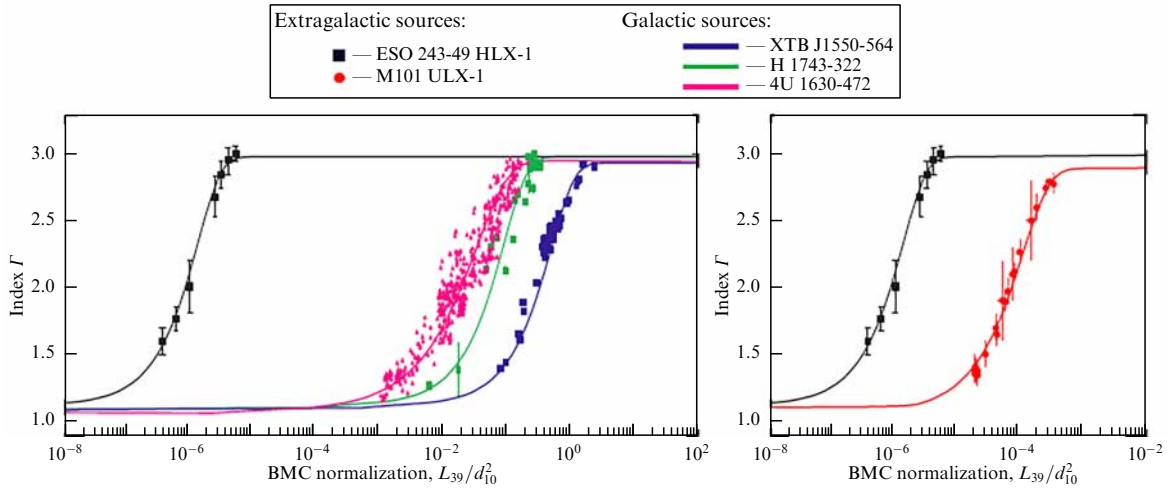

Figure 14. Correlation of the photon index with the accretion rate for extragalactic sources M101 ULX-1 and ESO 243-49 HLX-1 [56].

[23]). Thus, index saturation levels can vary from source to source, depending on the power of the soft photon flux arriving from the disk.

It is worth noting that the thermal Comptonization parameter $Y \sim [4kT/(m_e c^2)]\tau^2$, since, in this case, $\eta = 4kT/(m_e c^2)$ and $N_{sc} \sim \tau^2$ for $\tau \gg 1$ (see, for example, [55]), and thus the thermal Comptonization spectral index

$$\alpha \sim \left(\frac{4kT_e}{m_e c^2}\,\tau^2\right)^{-1}. \qquad (15)$$

2.6 Estimates of black hole masses for extragalactic sources

The same method described in Section 2.5 can also be used to estimate masses for extragalactic sources. Such a study using Swift/XRT data was carried out for ultraluminous sources M101 ULX-1 and ESO 243-49 HLX-1 (Fig. 14). The XTE J1550-564, H 1743-322, and 4U 1630-472 X-ray sources were used as reference sources. As a result, the BH masses were estimated to be $M_{BH} \sim 7 \times 10^4 M_\odot$ for ESO 243-49 and $M_{BH} \sim (3.2-4.3) \times 10^4 M_\odot$ for M101 ULX-1 [56, 57]. The color temperature of seed photons for these sources is in the range of 50–140 eV.

The scaling method was also applied to active galactic nuclei, namely to NGC 4051 [58]. In the analysis, GRO J1655-40 and Cyg X-1 were taken as reference sources. The correlations between the photon index and BMC normalization are shown in Fig. 15. Observational data were obtained by XMM-Newton, Suzaku, and RXTE. Study [58] also presented an analytical model showing that the photon index changes from a low value to relatively high values, depending on the accretion rate. The obtained mass value was $6 \times 10^5 M_\odot$.

Study [14] announced the discovery of correlations between the photon index and the accretion rate observed in the nuclei of the galaxies 3C 454.3 and M 87. The analytical model developed was used to show that Γ evolves from low to high values, depending on the accretion rate. Supermassive black holes (SMBHs) in NGC 4051 and NGC 7469 (see [59]) along with galactic BHs Cyg X-1 and GRO J1550-564 were used as reference sources to estimate the mass of the 3C 454.3 BH. For the masses of black holes in the central regions of the galaxies 3C 454.3 and M 87, the value obtained is

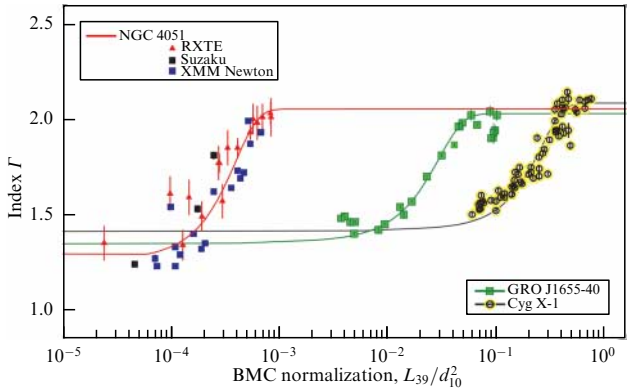

Figure 15. Correlation of photon index Γ with the BMC normalization. Red line corresponds to the studied source NGC 4051. Green and black lines refer to the reference sources GRO J1655-40 and Cyg X-1, respectively. Red triangles and black and blue squares show the data obtained by RXTE, Suzaku, and XMM-Newton, respectively [58].

$3.4 \times 10^9 M_\odot$ and $5.6 \times 10^7 M_\odot$, respectively. Recall that M87* is currently one of the two black holes (the other being SgrA*) (see Ref. [60]) whose masses have been estimated using radio interferometric measurements. For M87*, the mass turned out to be $6.5 \times 10^9\, M_\odot$. Such a large disagreement in the masses of the BHs at the center of the M87 galaxy, obtained by different methods, raises questions. The situation with the actual value of the mass of this BH will undoubtedly be clarified in the future.

2.7 High-temperature blackbody radiation in black-hole spectra. Shifted annihilation line

It was shown in [61] that broadband BH energy spectra contain a blackbody component with a temperature in the range of 15–40 keV (Fig. 16), which is called the High-Temperature BlackBody (HBB) component. It was studied in detail using observational data for five X-ray binaries: Cyg X-1, GX 339-4, GRS 1915+105, SS 433, and Sgr V4641 in low/hard, intermediate, high/soft, high, and very soft states, and using data on spectral transitions between them obtained by RXTE, INTEGRAL (INTErnational Gamma-Ray Astrophysics Laboratory), and BeppoSAX.

To fit these broadband spectra, an additive XSPEC model was used, which consists of Comptonized and Gaussian

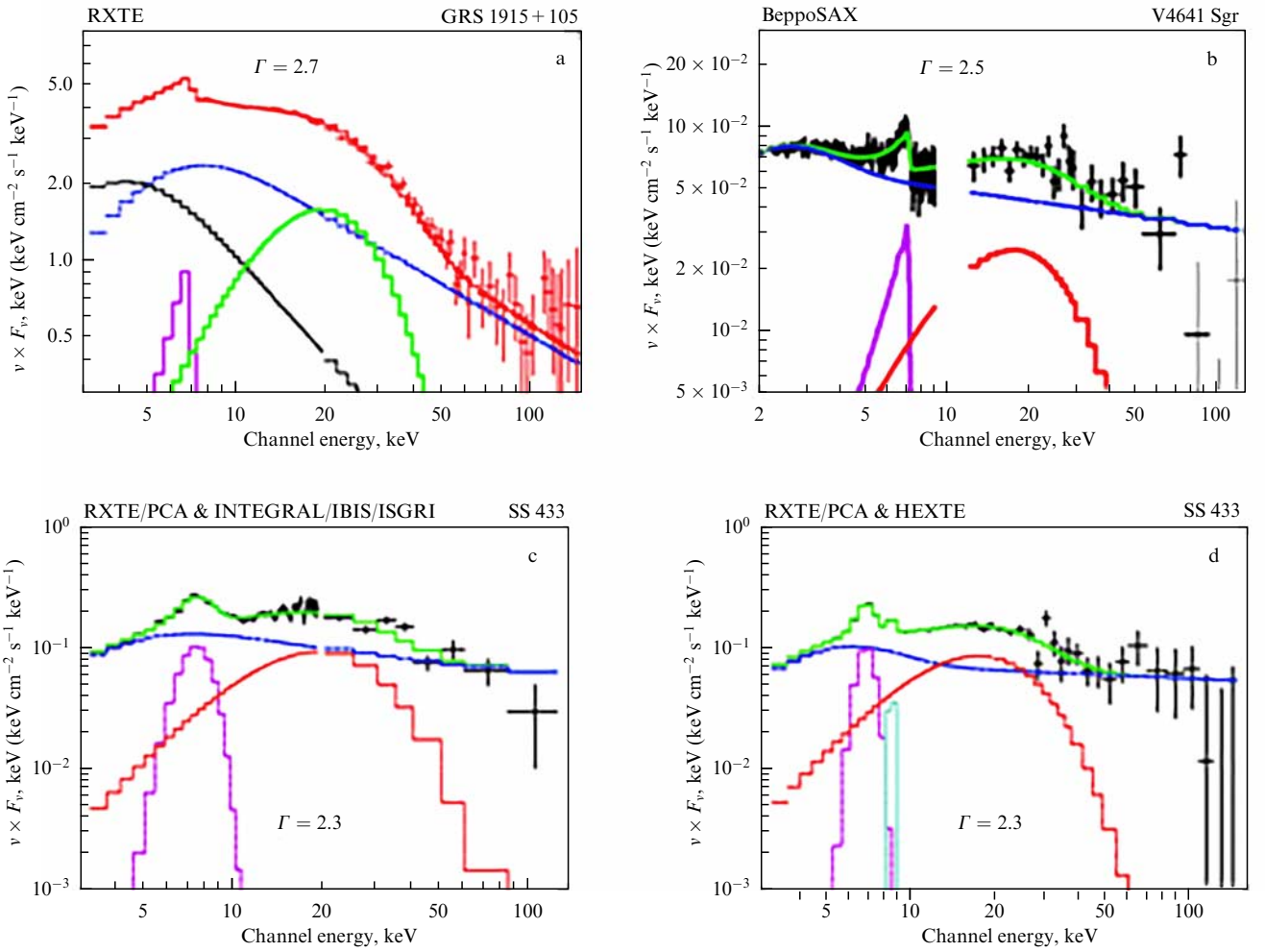

Figure 16. Results of calculations using the XSPEC model tbabs (comptb + gauss + bbody) smedge applied to spectra obtained by RXTE and BeppoSAX. Ordinates are $\nu \times F_\nu$, where ν is the photon frequency and F_ν is the spectral flux. Presence of a high-temperature blackbody component (gravitationally shifted annihilation line) is seen: green and red curves are for GRS 1915 + 105, SS 433, and V 4641 Sgr, respectively. Experimental data are shown as crosses; components of the spectral model are shown as a pink curve for the spectral line of iron (according to the relativistic Laor model in XSPEC) and as a blue curve for the Comptonization continuum (comptb-continuum). The resulting spectrum is represented by a red curve for GRS 1915 + 105) and green curves for SS 433 and V 4641 Sgr [61].

components. The study showed that, when the source was in the intermediate state, its spectrum contained an HBB component with a color temperature of $T_{\rm HBB}$ in the range of 4.5–5.9 keV. Using the data obtained with various X-ray telescopes, this component was detected only in some spectra of the five studied sources and only in the transition state (when the photon index $\Gamma > 1.9$).

The time scale of this spectral feature turned out to be several orders of magnitude smaller than that of the iron line and its edge, which implies that similar spectral features are formed in geometrically different parts of the source and in no way are related to each other. Previously, study [35] used numerical simulation to show the presence of a gravitationally shifted annihilation line in BH sources; therefore, the observed HBB bump in the BH spectra led to the assumption that the noted feature is a gravitationally shifted annihilation line. The equivalent width of the HBB singularity lies in the range from 400 to 800 eV (Fig. 17).

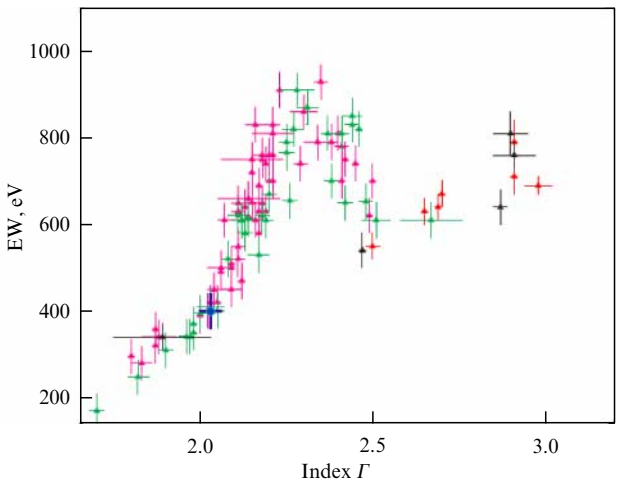

Figure 17. Equivalent width EW of a gravitationally shifted annihilation line as a function of the photon index. Points with error bars correspond to sources: Cyg X-1 (pink), GX 339 (green), GRS 1915 + 105 (red), and V 4641 Sgr (black) [61].

2.8 Discussion of the results of black-hole mass estimates

Currently, in X-ray observational astronomy, a compact object is identified as a BH based solely on its mass. A source

is classified as a BH if its mass exceeds the stability limit of a rotating neutron star, namely $3.2\,M_\odot$ (see, for example, [62]). To date, there is only one widely used method for determining the mass, associated with the measurement of the mass function $f(M)$, which is based on optical spectroscopy. Unlike the theoretical mass function, which is a combination of two masses and the orbit inclination angle, the observationally derived mass function, which sets a lower limit on the mass of a compact object, only depends on the radial velocity amplitude K and the orbital period $P_{\rm orb}$, and does not depend on the inclination angle i, i.e., $f(M) \propto P_{\rm orb}K^3$.

In [40], measurements of rotational velocities and inclinations for 17 binary systems containing black holes are collected. In many cases, the observed light curve is formed not only by the companion star but also by contributions from other radiation sources (usually the accretion disk). Another challenging aspect is the uncertainty of the radial velocity amplitude, which is contained in the solution in the third power.

Dynamic measurements of the mass of a compact object are more than the theoretical limit of a stable configuration. Note, however, that such a mass measurement is not direct evidence per se that the object under consideration is a black hole. Such evidence, for example, should originate from the confirmation of the presence of an event horizon for a BH. According to theoretical concepts, direct observations of the horizon are impossible. Therefore, it is necessary to look for such manifestations that require the presence of the horizon and thus may be proof of its presence. Section 2 presents theoretical arguments and observational evidence that the saturation of the photon index observed during spectral transitions in X-ray sources occurs due to dynamic Comptonization in a converging flow in the innermost region of a compact object. This region of a converging flow cannot be formed in the presence of a solid surface, which would observationally manifest itself as feedback in the form of a strong spectral component emerging due to the release of energy on the surface and coherent pulsations, for example, when the compact object is a neutron star. In fact, none of these features of the feedback has ever been observed in the case of X-ray sources, the compact object of which is assumed to be black holes. Therefore, we can assert with confidence that the observational fact of saturation of the photon index with an increase in the accretion rate is a unique property indicating the existence of a converging flow on a BH.

The table lists the values of the BH masses found using both dynamic methods and the scaling method. The mass values obtained by different methods are in good agreement. The BH masses found fall into a narrow range near $10M_\odot$, which may be due to some selection effect. Note that the scaling method has been fairly successfully used for extragalactic sources as well. In particular, for the ultraluminous sources M101 ULX-1 and ESO 243-49 HLX-1, we obtained black hole mass estimates $M_{\rm BH} \sim 7 \times 10^4 M_\odot$ and $M_{\rm BH} \sim (3.2-4.3) \times 10^4 M_\odot$, respectively.

2.9 Conclusions regarding estimation of black hole masses

We displayed an analysis of a representative set of observed spectral transitions in X-ray sources containing black holes with stellar masses. Spectral transition data for several galactic and extragalactic BHs obtained by RXTE and other missions, and correlations between the photon index Γ of the Comptonization component, its normalization, and the QPO frequency are presented.

Analyzing the behavior of correlation samples, four basic scaling laws can be formulated:

(1) inverse proportionality of the QPO frequency to the BH mass;

(2) proportionality of the X-ray flux from the disk to the BH mass;

(3) proportionality of the flux to the accretion rate;

(4) inverse proportionality of the flow to the distance from the source squared.

Combining correlation patterns for scaling of frequency and normalization datasets for a number of galactic X-ray binaries with BHs, the BH masses and distances to them were determined using the new independent method. The results obtained confirm that the scaling method is a powerful technique for determining BH masses. Applying the scaling method to determine BH masses with high accuracy requires very precise observations of source evolution during the burst and accurate scaling of reference sources.

The scaling method was tested using already known (from optical and IR observations and X-ray spectroscopic measurements) masses of BHs in 4U 15434-47, XTE J1859 + 226, XTE J1550-564, and Cyg X-1. Using the inverse proportionality of the QPO frequency to the BH mass for a given spectral state, we determined the masses of some BHs, which are in good agreement with the dynamically measured masses.

It is also shown that the transition layer model (see [1, 23]) makes it possible to fairly accurately predict the dependence of the frequency of quasi-periodic oscillations on the BH mass and the form of correlations between spectral and temporal properties observed during spectral transitions. The success of the scaling method for determining the BH masses provides important support for the assertion that the Compton cloud is the source of the observed correlation between the photon index and the QPO frequency. Indeed, the correlation between Γ and the QPO frequency (or accretion rate) arises from the fact that soft photons coming from the disk illuminate a fairly hot region adjacent to the source (transition layer), where these photons gain energy due to Comptonization.

We have presented observational evidence supporting the theory of the flow converging on a BH, since saturation of the photon index is observed with an increase in the accretion rate. As a result of the analysis, for example, of observations made by RXTE of a number of bursts near BHs, it was found that the saturation of the index is seen in the correlations between both the photon index and the QPO frequency and the photon index and the BMC normalization. We present arguments in favor of the fact that the saturation of the photon index with an increase in the accretion rate as a sign of a converging flow should always occur in the sources with BHs. It is only in such sources that there is no radiation pressure from the surface, similar to that observed in X-ray binaries with neutron stars, which occurs at a high accretion rate. In other words, the effect of saturation of the Γ index provides strong observational evidence of the existence of black holes in the X-ray sources under consideration.

A comparison of the black hole masses determined using dynamical methods with the mass values derived using the scaling method showed them to be in good agreement.

For extragalactic sources — ultraluminous X-ray (ULX) sources and active galactic nuclei (AGNs) — the existence of a correlation between the Γ index and the accretion rate and the saturation of the photon index is shown, which makes it possible to estimate masses of BHs contained in these objects.

It has also been shown that the spectra of some black hole candidates, Cyg X-1, GX 339-4, GRS 1915 + 105, SS 433, and V 4641 Sgc, contain a component of high-temperature blackbody radiation with a color temperature in the range of 4.5–5.9 keV, which is interpreted as a strongly redshifted annihilation line. This line is formed near the event horizon in a 200–300-m layer for a BH with a mass of $\sim 10M_{\odot}$.

3. Spectral characteristics of binaries with neutron stars. Constancy of the spectral index

The behavior of the spectral characteristics of radiation from systems containing neutron stars without significant magnetospheres can be analyzed using the X-ray source 4U 1728-34 as an example (see also [16]). A similar behavior of the spectral characteristics was also found in other sources, including NSs, such as 4U 1700-37 [63], 4U 1705-44 [64], Sco-X-1 [18], GX 340 + 0 [65], 4U 1820-30 [66], and GX 3 + 1 [67]. For such objects, during the transition from a high state to a low state, the temperature of electrons in the Compton cloud changes from 2.5 to 15 keV. Thus, a high spectral state corresponds to one with a low electron temperature. During a burst visible in the ASM (All-Sky Monitor) light curve, the electron temperature T_e decreases from 15 to 2.5 keV. A detailed data analysis can be found in [16]. The data used, which are publicly available, can be found in the GSFC (Goddard Space Flight Center) archive.[10]

3.1 Spectral analysis

The spectral analysis in [16] used a model consisting of a Comptonization (COMPTB) component (see [9]), a blackbody component with a characteristic temperature T_{BB}, and a Gaussian one describing the ionized-iron line. The parameters of the COMPTB spectral component are the temperature of the seed photons T_s, the energy index of the Comptonization spectrum α, the electron temperature T_e, the Comptonization fraction f, presented in the conventional form as $f = A/(1 + A)$, and the normalization of seed photons N_{COMPTB}.

Figure 1 illustrates the source structure. Matter accreting onto a neutron star without a significant magnetosphere arrives from two regions: a geometrically thin accretion disk, which can be represented, for example, by a Shakura–Sunyaev disk [33], and a transition layer, where soft photons emitted from the disk and the neutron star surface gain energy on the hot electrons of the Compton cloud. Thus, as in the case of X-ray sources with black holes, the resulting Comptonization spectrum is formed in the transition layer, where photons from the disk and neutron star, which initially have soft X-ray temperatures, gain energy in the hot plasma. Some fraction of these soft photons can be directly observable.

Figure 18 (according to RXTE data [16]) displays the X-ray spectrum of 4U 1728-34 (see also [16] for BeppoSAX data). The analysis shows that the X-ray spectrum of 4U 1728-34 can be described by the Comptonization model, and its component of the same name can be represented by the COMPTB model. For broadband BeppoSAX observations, this spectral component is modified at low energies by photoelectric absorption. Also, following [68, 69], to improve the fitting statistics, a Gaussian can be added at an energy of 6.7 keV and a thermal blackbody component in the low energy range (1–4 keV). Along with these components, the authors of [68] included a narrow Gaussian line in the spectral model to take into account the excess in the residual deviations near energies of 1.7 keV. In [16], the possible presence of this line was tested to show that its addition does not improve the quality of the model fit. It should be noted that study [70] analyzed the simultaneous observations made on March 2–5, 2002 for 4U 1728-34 by Chandra and RXTE. The continuum was fitted in the range of 1.2–35 keV by the sum of the blackbody and Comptonization components, and large residual deviations in the range of 6–10 keV were fitted by a wide (with the equivalent full width at half maximum width (FWHM) ~ 2 keV) Gaussian emission line or, alternatively, two absorption edges associated with low-ionized iron and Fe XXV/XXVI. The authors of [16], using the wabs*(blackbody + COMPTB + Gaussian) model, found signs of an iron line in all observations made by BeppoSAX and RXTE.

An analysis of the BeppoSAX data for this source (see [10]) showed that the spectral index remains constant, $\alpha = 1.03 \pm 0.04$. At the same time, the temperature of soft photons T_s for the COMPTB component increases from 1.2 to 1.3 keV, and the color temperature of the soft blackbody component T_{BB} varies around 0.6 keV.

Unfortunately, RXTE detectors cannot provide well-calibrated spectra at energies below 3 keV, while the wide energy range of the BeppoSAX telescopes makes it possible to determine the parameters of soft blackbody components. Thus, to approximate the data obtained by RXTE, it is necessary to fix the temperature of the blackbody component at a level of $T_{BB} = 0.7$ keV, obtained as an upper limit using the BeppoSAX data.

The electron temperature T_e of the COMPTB component varies from 2.5 to 15 keV, while the photon index Γ remains almost constant ($\Gamma = 1.99 \pm 0.02$) for all observations, and the width of the Gaussian component varies within 0.3–0.6 keV. The color temperature T_s of the COMPTB component remains close to 1.3 keV, which agrees with the value obtained using the BeppoSAX data and previously obtained results [68, 69].

The important parameter COMPTB can be fixed at the level $f = 1$, when, by virtue of the accepted definition $f = A/(1 + A)$, the value of $\log A \gg 1$. In further calculations, the value of the hydrogen column can be set equal to $N_H = 2.73 \times 10^{22}$ cm^{-2} [69]. Figure 18 illustrates the best fit of the RXTE spectrum for 4U 1728-34 in the low state. The parameters of the best model fit for these observations are $\Gamma = 1.99 \pm 0.02$, $T_e = 10.4 \pm 0.3$ keV, and $E_{line} = 6.54 \pm 0.03$ keV.

The same procedure can be applied to the spectrum of a source in a high state; its results are given in [16]. The parameters of the best fit of the model in this case are $\Gamma = 1.99 \pm 0.02$, $T_e = 5.5 \pm 0.1$ keV, and $E_{line} = 6.75 \pm 0.04$ keV. The adopted spectral model yielded very good results for all data used in the analysis. Note that the value of χ^2/N_{dof}, where N_{dof} is the number of degrees of freedom, is close to 1.0 for most observational data.

An analysis of high-resolution spectra obtained by XMM-Newton for 4U 1728-34 [71, 72] using various spectral models also showed significant discrepancies in the 6–7 keV range due to the presence of a broad emission line. Note the difference between the values of the same parameters in different models. In particular, the photon index Γ estimated

[10] http://heasarc.gsfc.nasa.gov.

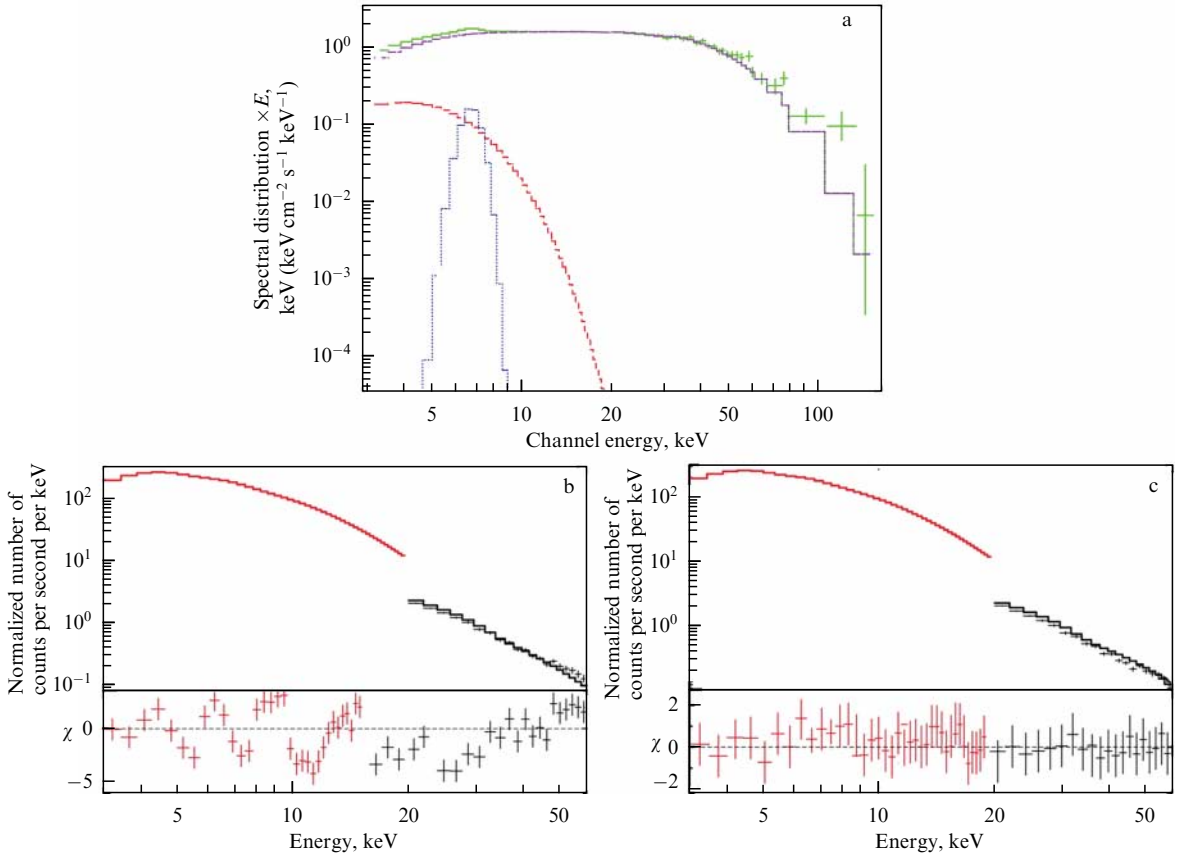

Figure 18. Best approximation of the 4U 1728-34 spectrum for the low state in energy units (a) and counts (b, c) with residual deviations $\Delta\chi$ for observation 30042-03-01-00 by RXTE. Red, purple, and blue lines represent the blackbody component, COMPTB, and Gaussian, respectively. (b) Approximation and residual deviations for the wabs∗COMPTB model. (c) Same as in panel b, but with the addition of a Gaussian iron line and a blackbody component, namely, using the wabs∗(blackbody + COMPTB + Gaussian) model. Best approximation parameters are $\Gamma = 1.99 \pm 0.02$, $T_e = 10.4 \pm 0.3$ keV, and line $E_{line} = 6.54 \pm 0.03$ keV [16].

in [73] for the observation ObsID = 20674001 was 1.60 ± 0.25, while in [16], $\Gamma = 1.9 \pm 0.2$. This difference in index values can be explained by the use of different spectral models: in [68], a narrow Gaussian line of about 1.7 keV (recombination emission of Mg XI) was included to eliminate the excess of the residual deviations of the continuum model. In [16], a slightly different model was applied. The value of the photon index $\Gamma = 1.9 \pm 0.2$ is very close to that obtained in [69], where the fit to the observed spectrum was carried out by the COMPTT model (see [6]); as a result, the values of the electron temperature $T_e = 3.16 \pm 0.03$ keV and optical depth (for spherical geometry) $\tau_0 = 11.4 \pm 0.2$ were obtained.

3.2 Evolution of X-ray spectral properties during spectral transitions

Figure 18 (see also [16]) displays typical examples of the 4U 1728-34 spectra observed by RXTE in the low and high states. As can be seen, the normalization of the thermal blackbody component is twice as high in the high state as in the low state, although the photon indices Γ for each of these spectra vary only slightly from 1.8 to 2.1, localizing around $\Gamma = 2$ (see the distribution of Γ in Fig. 19). It is of importance to emphasize that the index Γ does not depend on the plasma temperature of the Compton cloud T_e (see [16]). Using the BeppoSAX data, the authors of [15] assumed that the value of Γ is close to 2 for a sufficiently large number of X-ray sources containing a neutron star. The spectral state of such a system is characterized by electron temperature T_e, and, as the authors of [15] show, $\Gamma = 2 \pm 0.2$ (or $\alpha = 1 \pm 0.2$) when T_e varies from 2.5 to 25 keV.

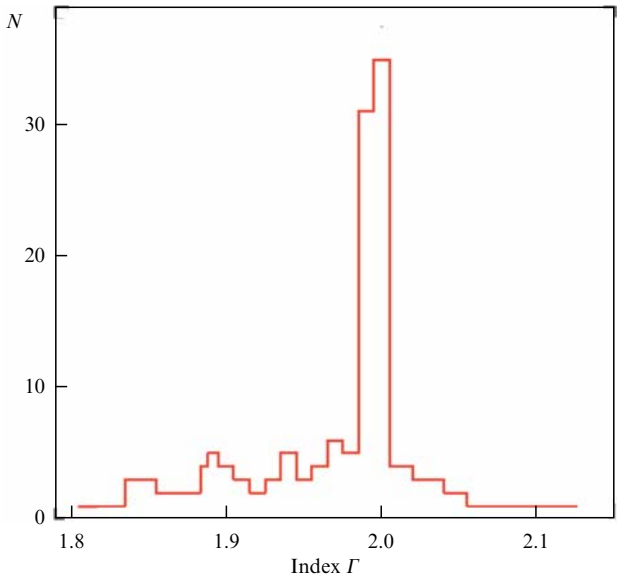

Figure 19. Histogram of the distribution of index Γ for the source 4U 1728-34 [16].

In 1998–2000, RXTE detected a sizable number of X-ray bursts with good coverage of rise/decay transitions for source 4U 1728-34.

An analysis of the observations shows that, in the case of neutron stars, as the flux of soft disk photons increases, the temperature T_e of the Compton cloud decreases, a well-known effect that was explained in [1, 23]. In most cases, the soft disk emission in 4U 1728-34 is processed in the Compton cloud, and only a small fraction of the flux from the disk $(1-f)$ is directly visible to a terrestrial observer. Thus, the energy spectrum of the 4U 1728-34 source in all states is due to the Comptonization component, while the direct disk emission is always weak and only visible during a burst (see [16]).

Note that the determination of the spectral transition for a BH is related to the change in the photon index Γ (see, for example, [13]). However, there is no direct correspondence between Γ and the energy of the exponential dip. Study [74], based on the analysis of RXTE data for a binary system containing XTE J1550-564 BH, showed that the energy of the dip decreases with an increase in Γ from 1.4 to 2.1–2.2, and only after Γ reaches 2.2 does the energy of the dip also increase. Thus, for X-ray systems containing black holes, the main parameter used to describe the spectral transition is the variable photon index Γ, which increases monotonically when the source with a BH evolves into a high/soft state.

It is of importance to emphasize that in 4U 1728-34, a binary system with a neutron star, the transition from a low state to a high state occurs when the electron temperature decreases from 15 to 2.5 keV. Thus, following the assumption made in [15], the spectral transition of states in a source with a NS can be determined using the electron temperature T_e of the Compton cloud. In this case, the low state is characterized by a high temperature T_e, while the high state is associated with a lower T_e value. Note that T_e is a directly measurable quantity and corresponds to the cutoff energy in the source spectrum.

Bursts only occur in a few X-ray systems containing neutron stars. However, such events make it possible to establish a significant difference between an NS and a BH. During the burst, the source evolves from a low state to a high one, and the plasma temperature of the Comptonization region changes significantly, similar to the plasma temperature in the 4U 1728-34 source, where it rises from 2.5 to 15 keV. Thus, when the source returns from a low to a high state, the temperature T_e decreases, while the photon index Γ remains close to 2. In systems with a BH, a steady monotonic increase in Γ is seen, which is not observed in systems with a NS, and ends with saturation of the index (see, for example, [13]).

3.3 Correlation between spectral and temporal properties during spectral transitions

Figure 20 presents the typical evolution of the temporal and spectral characteristics of X-rays during bursts. The evolution of RXTE/ASM signal counts during the 1998 burst is shown in Fig. 20a. The red/blue dots A, B, and C mark the moments MJD = 51,122/51,128, 51,133.27/51,133.34, and 51,196/51,193 before, during, and after the X-ray burst, respectively. Figures 20b–d show the power spectra for the energy range of 13–30 keV along with the spectral diagram $EF(E)$ for X-ray light curve points A (Fig. 20e), B (Fig. 20f), and C (Fig. 20g).

Strong noise components with a kink at 1–3 Hz and wide QPOs concentrated in the 7–10 Hz region are visible both before and after the burst, but the QPOs disappear during the peak of the X-ray burst (Fig. 20c). During the B1 burst, a noise component can be seen with a peak shifted to high frequencies relative to the A1/C1 events. In other words, the power spectra during the burst consist of high-frequency red-white noise with a kink around 40 Hz. Figures 20e–g show the spectral diagrams associated with the corresponding power spectra (Fig. 20b-d). The data are shown as red dots, and the spectral model components are presented as solid blue, black, and dashed purple lines for the Comptonization, blackbody, and Gaussian components, respectively.

In particular, before the burst (A1 red, RXTE 30042-03-08-00, MJD = 51,122), a noise component can be seen with a power-law spectrum and with a kink at 1 Hz and a wide QPO at 20 Hz, described by a Lorentzian with FWHM $= 11.7 \pm 4.5$ Hz, rms $= 6.3 \pm 1.0\%$, and $\chi^2 = 131$ for 102 degrees of freedom at a 67% confidence level. Later (A1 blue, 30042-03-11-00, MJD = 51,128), the kink frequency in the power noise component shifts from 1 to 3 Hz, and the presence of QPOs becomes less visible, although they are still seen in the range of 10–20 Hz. The low frequency part of the $\nu \times power$ diagram (below 1 Hz) rises before the burst (Fig. 20b, blue curve). During the burst (Fig. 20c, red curve, 30042-03-14-02, MJD = 51,133.27; Fig. 20c, blue curve, 30042-03-14-01, MJD = 51,133.34), white-red noise can be seen with a kink frequency shifted to a higher frequency, about 40 Hz. This QPO component is not visible in the power spectrum during the burst at frequencies of 80 Hz or below.

A similar behavior, which can be called a 'burst transition,' was also detected earlier for 4U 1728-34 (see [75]) during the 1996–1997 transition from the 'island' state to the 'banana' state in the diagram (see Fig. 1 in [75]). Note that, according to [75], the power spectrum in the upper 'banana' state (during the burst maximum) consists of two noise components, namely, low-frequency and high-frequency.

After the burst (Fig. 20d, blue curve, 30042-03-18-00, MJD = 51,193; Fig. 20d, red curve, 30042-03-20-00, MJD = 51,196), the same features can be seen on the $\nu \times power$ diagram as before the burst, but with shifted values of the parameters: $\nu_{br} \sim 1$, 2 Hz and $\nu_{QPO} \sim 6$, 10 Hz (described by the Lorentzian profile with FWHM $= 6.0 \pm 2.1/15.0 \pm 2.9$ Hz, rms $= 8.1 \pm 0.4/10.6 \pm 1.4\%$, and $\chi^2_{red} = 139/143$ for 102 degrees of freedom (all errors correspond to the 1σ confidence interval)).

For comparison, study [16] presents the $\nu \times power$ diagram obtained on March 7, 2000 (50023-01-01-00 RXTE, MJD = 51,610) in the quiescent state (compare with Fig. 20c).

3.4 Discussion

Thus, in the source 4U 1728-34, a constancy of the photon index was found in all observations. In [16], the index Γ is shown to correlate with the COMPTB normalization (which is equal to the normalization of blackbody photons) and the fraction of Comptonized photons f. These results are obtained 'from first principles.' This stability of the index, which was also revealed in observations of other X-ray binaries with an NS, was explained in terms of the transition layer concept [15].

The energy balance in the transition layer is due to Coulomb collisions of protons (release of gravitational energy), while inverse Compton emission and free-free transitions are the main cooling channels [76, 77].

For the characteristic range of electron temperature ($3 \leqslant T_e \leqslant 30$ keV) and characteristic density values ($\leqslant 10^{-5}$ g cm^{-3}) in these regions in low-mass X-ray binaries,

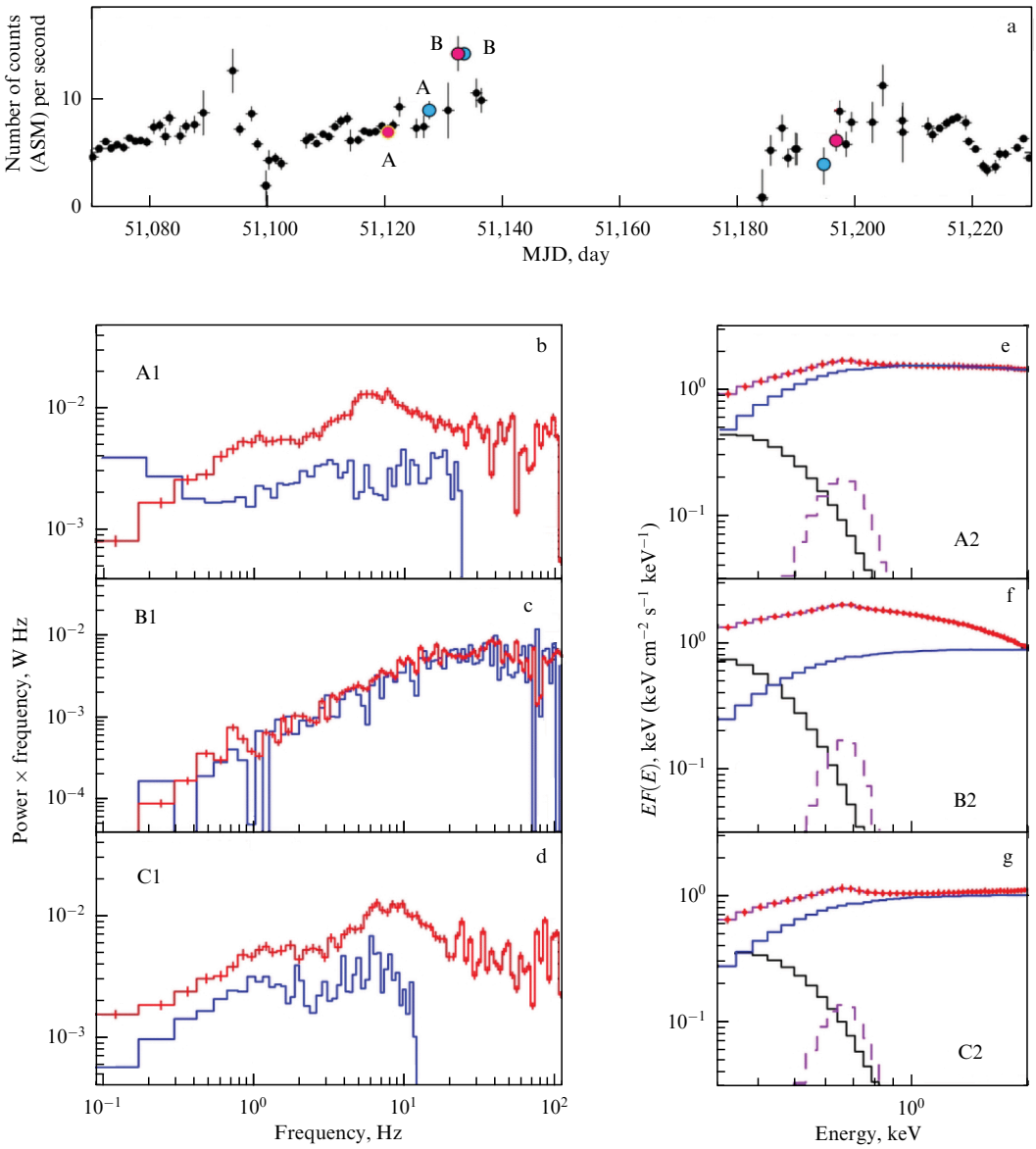

Figure 20. (a) RXTE/ASM count rate during the 1998–1999 burst transition (R3, R5). Red/blue dots A, B, and C mark the moments at MJD = 51,122/51,128, 51,133.27/51,133.34, and 51,196/51,193 (before, during, and after the X-ray burst, respectively) (MJD is the modified Julian date), (b–d) PDS for the energy range of the 13–30 keV band plotted together with the energy spectral diagram $EF(E)$ (e–g) associated with points A, B, and C of the X-ray light curve in panel a. Strong noise component due to discontinuity at 1–3 Hz and wide QPOs centered at a frequency of 7–10 Hz are present before and after the burst (see panels b and d). At the peak of the X-ray burst (panel c), white-red noise is seen with a pause at 40 Hz. Spectral diagrams $EF(E)$ shown in panels e–g are related by the corresponding power spectra displayed in panels b–d. Data are shown with red symbols, and the components of the spectral model are shown with solid blue and black lines and dashed purple curves for the COMPTB component, blackbody component, and Gaussian component, respectively [16].

Compton cooling prevails over free-free emission; the relation between the energy flux per unit corona surface $Q_{\rm cor}$, the radiation energy density $\varepsilon(\tau)$, and the electron temperature $T_{\rm e}$ (see also [1]) has the form

$$\frac{Q_{\rm cor}}{\tau_0} \sim 20.2\varepsilon(\tau)T_{\rm e}(\tau)\,, \tag{16}$$

where τ_0 is the Thomson optical depth of the transition layer. The distribution $\varepsilon(\tau)$ was obtained as a solution to the diffusion equation

$$\frac{{\rm d}^2\varepsilon}{{\rm d}\tau^2} = -3\,\frac{Q_{\rm tot}}{c\,\tau_0}\,, \tag{17}$$

where $Q_{\rm tot} = Q_{\rm cor} + Q_{\rm disk}$ is the sum of the flux from the corona and the flux intercepted from the disk. Combining Eqn (17) with two boundary conditions on the NS surface and on the outer boundary of the transition layer,

$$\left.\frac{{\rm d}\varepsilon}{{\rm d}\tau}\right|_{\tau=\tau_0} = 0\,, \tag{18}$$

$$\left.\left(\frac{{\rm d}\varepsilon}{{\rm d}\tau} - \frac{3}{2}\,\varepsilon\right)\right|_{\tau=0} = 0\,, \tag{19}$$

leads to the formulation of the transition layer problem [15].

Boundary condition (18) implies that photons incident on the NS surface are completely reflected; in other words, the albedo $A = 1$ at the inner boundary of the transition layer,

$\tau = \tau_0$. Boundary condition (19) at $\tau = 0$ is associated with the absence of diffusive (scattered) radiation incident from the outside on the intermediate layer (transition layer, corona). Thus, the solution for $\varepsilon(\tau)$ can be represented as

$$\varepsilon(\tau) = \frac{2Q_{\rm tot}}{c}\left[1 + \frac{3}{2}\,\tau_0\left(\frac{\tau}{\tau_0} - \frac{\tau^2}{2\tau_0^2}\right)\right]. \qquad (20)$$

To find the average plasma temperature $T_{\rm e}$, it is necessary to estimate the average energy density in the transition layer:

$$\left\langle \varepsilon(\tau)\right\rangle = \frac{1}{\tau_0}\int_0^{\tau_0} \varepsilon(\tau)\,{\rm d}\tau = \frac{Q_{\rm tot}}{c}(2+\tau_0)\,. \qquad (21)$$

If the result that follows from Eqn (21) is substituted into Eqn (16), after simple algebraic transformations, we obtain

$$\frac{kT_{\rm e}\tau_0(2+\tau_0)}{m_{\rm e}c^2} = \frac{0.25}{1+Q_{\rm disk}/Q_{\rm cor}}\,. \qquad (22)$$

It is also necessary to use the following formula for the spectral index α:

$$\alpha = -\frac{3}{2} + \sqrt{\frac{9}{4} + \frac{\beta}{\Theta}},$$

where $\Theta \equiv kT_{\rm e}/(m_{\rm e}c^2)$ and β is the parameter defined in [8]. If we replace the function β by its diffusion limit $\beta_{\rm diff}$,

$$\beta_{\rm diff} = \frac{1}{\tau_0(2+\tau_0)}\,,$$

then, using Eqn (22), we obtain the diffusive spectral index

$$\alpha_{\rm diff} = -\frac{3}{2} + \sqrt{\frac{9}{4} + \frac{1+Q_{\rm disk}/Q_{\rm cor}}{0.25}}$$

or $\alpha_{\rm diff} \sim 1 + 0.8\,Q_{\rm disk}/Q_{\rm cor}$ and

$$\Gamma_{\rm diff} \sim 1 + \alpha_{\rm diff} = 2 + 0.8\,\frac{Q_{\rm disk}}{Q_{\rm cor}}$$

for $Q_{\rm disk}/Q_{\rm cor} \ll 1$. Thus, as long as $Q_{\rm disk}/Q_{\rm cor} \ll 1$, the photon index $\Gamma \sim 2$; exactly this is observed in 4U 1728-34 (see Fig. 19).

The observational data on black holes show that the photon index increases monotonically with an increase in the QPO frequency and the accretion rate and, saturating, becomes constant (see [13, 78, 79]). In [35], the formation of X-ray spectra in a Compton cloud surrounding a BH was simulated using the Monte Carlo method. The authors successfully reproduced the observed correlations between the index and the accretion rate. It was also shown that the index saturation in the BH is the result of two effects, namely, the cooling of the converging flow into the BH by soft photons coming from the disk and the capture of photons by the black hole. Indeed, the spectral index α is inversely proportional to the Comptonization parameter Y, which in turn is proportional to the average number of effective scatterings (upscattering) $N_{\rm sc}$ and the energy gain efficiency η.

However, in a relatively cold converging flow, when the accretion rate $\dot{m} \gg 1$, photons are scattered by electrons in the direction of the flow, in which the number of scatterings $N_{\rm sc}$ is proportional to the optical depth $\tau_{\rm CF}$ (or $\dot{m}$), and η is inversely proportional to $\tau_{\rm CF}$. Thus, the spectral (photon) index saturates when the accretion rate increases, which was reproduced in Monte Carlo simulations in [35]. Therefore, we can conclude that the monotonic increase in the photon index with the accretion rate that follows the saturation of the index is an observable signature of the BH, while the constancy of Γ (about 2) with respect to $\dot{m}$ (or electron temperature) is a characteristic feature of a neutron star.

The authors of [80] found that in ultraluminous X-ray sources (HLX1) the photon index varies from 1.8 to 2.95, but failed to find arguments to conclude whether this source is an intermediate-mass BH or NS. A comparison of the results of [15] and [16] for an NS and the results of [13] for a BH (see also [35]) shows that HLX1 is apparently a BH, since the photon index of this source varies over a wide range from 1.8 to 2.95, while in the NS case the index would not change and would remain almost constant, close to 2 (see, for example, Fig. 19).

3.5 Conclusions

Thus, X-ray broadband energy spectra for all spectral states can be adequately approximated by the sum of the Compton (COMPTB), blackbody, and Gaussian components. Figure 21 shows examples of plots of the dependence of the photon index Γ on the accretion rate for the BH sources GRS 1915+105 [78], GX 339-4 [13], and SS 433 [79], and for the neutron star 4U 1728-34. As can be seen, the index Γ for BH sources first increases and then saturates (moreover, the saturation level changes from source to source), while, for 4U 1728-34 NS, Γ remains almost unchanged and varies in a narrow range of about 2 (see also Fig. 19). The photon index Γ for the best fittings of the Compton component in 4U 1728-34 remains almost constant, close to 2, and depends neither on the L_{39}/d_{10}^2 normalization of the COMPTB, which is proportional to the accretion rate in the disk $\dot{m}$, nor on the plasma temperature of the Compton cloud $T_{\rm e}$ (see [16]).

The luminosity of the soft (coming from the disk) photon component L_{39} is presented in units of 10^{39} erg s^{-1} and the distance to the source d_{10}, in units 10 kpc. The stability of the index was also initially discovered for a number of other sources, where the X-ray emission of the system is formed near the NS it contains: Cyg X-2, Sco X-1, GX 17+2, GX 340+0, GX 3+1, GX 349+2, X 1658-298, GS 1826-238, and 1E 1724-3045, which were observed by BeppoSAX in various spectral states (see details in [15]). It was revealed that these sources are characterized by a relatively high value of the Comptonization fraction, $f = 0.6-0.9$, obtained in the spectral model considered in [16], which, in turn, indicates a significant processing of disk emission in the Compton cloud in 4U 1728-34. Based on the observational data obtained by BeppoSAX, it is also found that black body radiation originates from two sources. One of them (with a temperature of about 0.7 keV) is apparently associated with the accretion disk, while the other, with the NS surface itself (1.3 keV).

The photon index for neutron stars remains constant at ~ 2 when the source evolves from a low spectral state to a high one, in other words, when the plasma temperature of the Compton cloud changes from 2.5 to 15 keV (see [16]). We present theoretical arguments in favor of the assertion that, if the release of gravitational energy in the transition layer dominates over the flux of soft photons coming from the accretion disk, i.e., $Q_{\rm disk}/Q_{\rm cor} \ll 1$, this leads to an almost constant photon index $\Gamma \simeq 2$.

Thus, the constancy of the photon index is an intrinsic property of an X-ray binary with an NS, while, in systems where a BH is a compact object, the index changes monotonically with the accretion rate and then saturates.

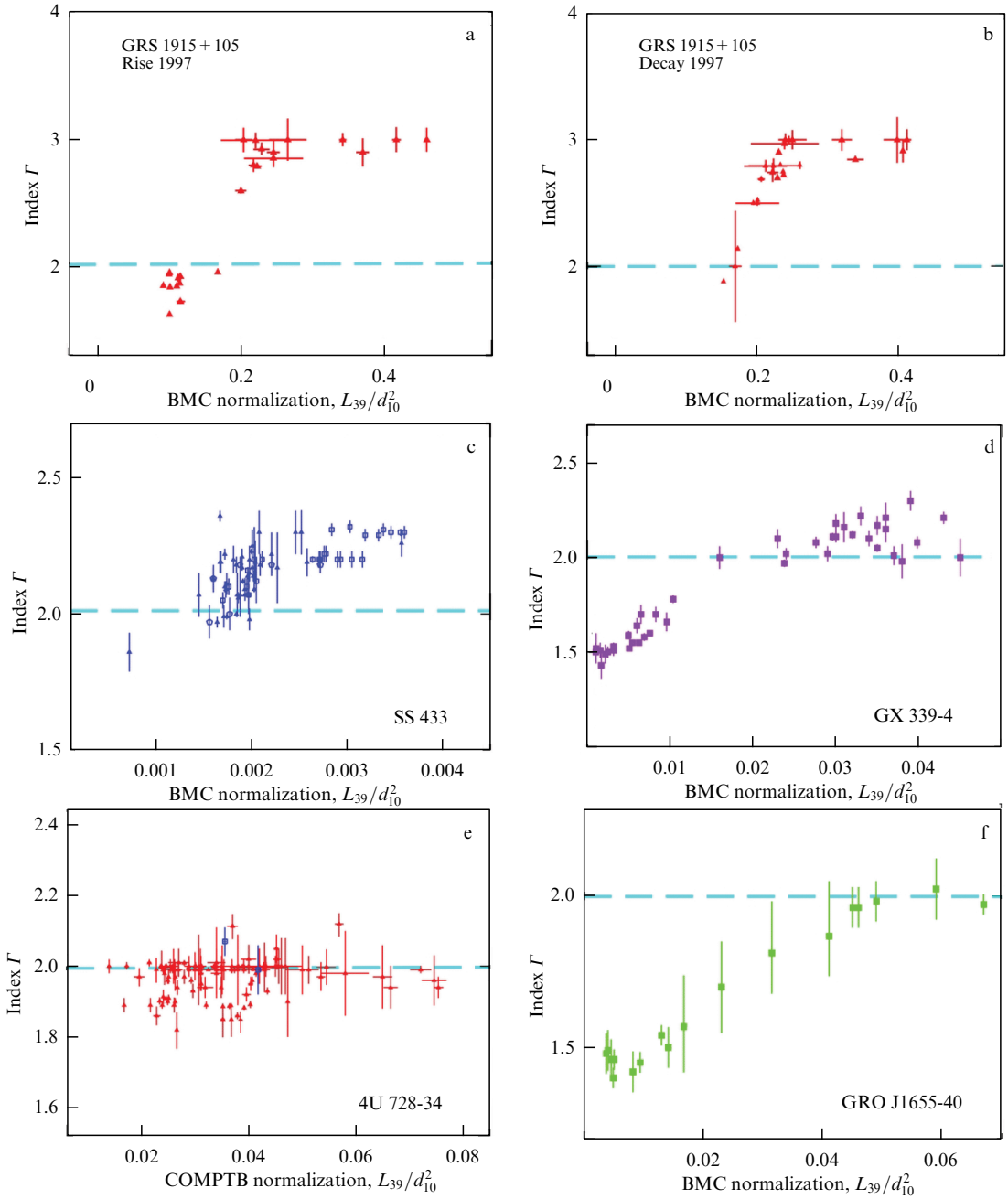

Figure 21. Examples of plots of photon index Γ vs. accretion rate for sources GRS 1915 + 105 [78], GX 339-4 [13], SS 433 [79], and GRO J1655-40 [13] and for 4U 1728-34. Level $\Gamma = 2$ is indicated by a blue dashed line.

4. White dwarfs as X-ray sources

We now briefly review results on the study of the X-ray spectral continuum of nonmagnetic cataclysmic variables (nmCVs) using as an example four nmCVs: U Gem, SS Cyg, VW Hyi, and SS Aur, which are among the brightest sources of this type. The observational basis for the analysis consists of the data obtained by XMM-Newton Epic-pn, Chandra HETG/ACIS, LETG/HRC, RXTE PCA, and HEXTE (High-Energy X-ray Timing Experiment).

4.1 Data description

4.1.1 HMM-Newton. Study [81] analyzed four sets of publicly available observational data obtained with the XMM-Newton EPIC-pn instrument, one observation for each source. All XMM-Newton observations were made when the sources were in the quiescent state.

VW Hyi, U Gem, and SS Aur were observed using the pn camera operating in Imaging mode, while SS Cyg was observed with the pn-camera in Timing mode. All light curves and spectra were plotted using Science Analysis Software (SAS), version 14.0.0.

4.1.2 Chandra. Eight publicly available sets of Chandra observations were used for the analysis. VW Hyi was observed only once during the burst, while SS Cyg and U Gem were observed four and three times, respectively, both during the burst and in the quiescent state. The data archive contains no observations of SS Aur. SS Cyg, U Gem, and VW Hyi were observed once in LETG/HRC-S mode,

while SS Cyg and U Gem were observed thrice and twice in HETG/ACIS-S mode, respectively. For each observation, two light curves were extracted in the 0.4–4 keV and 4–10 keV bands and tested for variability. Significant changes in the hardness of the spectra were not observed; therefore, the total exposure time was used to reproduce the observed spectra.

4.1.3 RXTE. Six RXTE observations of three nmCVs were analyzed: one for U Gem, one for SS Aur, and four for SS Cyg. SS Aur and SS Cyg (Obs. ID 50012-01-01) were observed in the quiescent state. All other observations were made when the source was in the burst state. PCA data were analyzed according to the standard procedure using RXTE/FTOOLS tools.

4.2 Spectral analysis

To test the results of fitting the Comptonization model to data specifically for nmCVs and to obtain more accurate estimates of the physical parameters and spectral parameters in these systems, the authors of [81] analyzed data obtained at three observatories: XMM-Newton, Chandra, and RXTE. The observational data were analyzed using the XSPEC astrophysical package.

The spectral continuum was first modeled by a single thermal Comptonization component, the COMPTT model in XSPEC [6–8], with a planar geometry of the plasma cloud. The fitting parameters of the model are the seed photon temperature T_s, the electron temperature T_e, and the optical depth of the Compton cloud τ. The second Comptonization component was added to the general model only when it was required for fitting, which occurred in three of the four spectra of SS Cyg.

All spectra provided by XMM-Newton, Chandra, and RXTE exhibit a residual excess associated with emission lines from the K-shell of Fe XXI–XXVI ($\sim 6.4-7.0$ keV). The spectrum was modeled using three Gaussian components. Due to the low energy resolution of RXTE/PCA, only one (wide) line was used.

4.2.1 Spectral analysis of XMM-Newton. The addition of photoelectric absorption (N_H) and/or a blackbody component (for example, in the BBODY or BBODYRAD model) does not improve the quality of fitting for any XMM-Newton spectra in the energy range of $\sim 0.3-15/0.4-10$ keV.

The U Gem spectrum showed the presence of three iron emission lines centered at energies $6.394^{+0.013}_{-0.013}$ keV, $6.68^{+0.04}_{-0.04}$ keV, and $6.972^{+0.023}_{-0.019}$ keV, with equivalent widths (EWs) of 53^{+41}_{-25} eV, 281^{+100}_{-49} eV, and 167^{+53}_{-40} eV, respectively. The spectra of SS Cyg and SS Aur exhibited two iron emission lines. In SS Cyg, the lines are centered at energies of $6.634^{+0.026}_{-0.023}$ keV (compatible with the neutral iron line K_α) and $6.966^{+0.030}_{-0.026}$ keV (1.1σ from the H-like iron line K_α at 7.0 keV) and have equivalent widths of 186^{+321}_{-27} eV and 75^{+97}_{-20} eV, respectively. In SS Aur, the central energy values are $6.67^{+0.04}_{-0.03}$ keV (compatible with the He-like line of iron K_α) and $7.00^{+0.05}_{-0.05}$ keV (compatible with the H-like line of iron K_α); the equivalent widths are 528^{+388}_{-156} eV and 169^{+99}_{-89} eV, respectively. The VW Hyi spectrum was the only one that showed a single iron emission line. The energy of its Gaussian centroid is $6.672^{+0.017}_{-0.015}$ keV (1.6σ away from the He-like iron line of K_α), and the line is very strong: its equivalent width is 995^{+152}_{-143} eV, several times greater than in other sources.

The parameters of the model spectra found for each XMM-Newton observation exhibit the presence of Gaussian iron lines [81]. In addition to the emission lines of iron in the energy range of 6.4–7.0 keV, all spectra also exhibit another strong and broad residual excess, which reaches a maximum at ~ 1.01 keV, with a Gaussian centroid in the range of $\sim 0.96-1.02$ keV. The noted properties make it possible to interpret these lines as resonance lines associated with Ne X, Fe XVII, or Fe XXL ions.

Thus, the physical parameters of the COMPTT model lie in the following range:

- temperature T_s of seed photons ranges from 0.056 to 0.174 keV;
- temperature of electrons T_e in the Comptonization cloud ranges from 5.99 to 8.72 keV;
- optical depth τ of this cloud ranges from 2.65 to 4.73.

4.2.2 Spectral analysis of Chandra data. In all studied spectra, a residual wide excess near an energy of 1 keV was detected, which was also observed in three of the five HETG/ACIS Chandra spectra. For U Gem, the values of the parameters τ and T_e at a 90% confidence level are $\tau \sim 5$ and $T_e = 5.0^{+0.5}_{-0.5}$ keV in the quiescent state (Obs.647) and 6^{+5}_{-2} keV in the active state (Obs.3767). The temperature T_s of seed photons in the Obs.3767 observation is $0.66^{+0.12}_{-0.10}$ keV, which is ~ 8 times higher than that obtained in the analysis of the Obs.647 observation.

In SS Cyg, the best fitting was usually obtained using the COMPTT component, for which $T_s = 0.10$ keV, $T_e \sim 5$ keV, and $\tau \sim 6$. The electron temperature either exceeds the upper limit specified by the effective energy band of Chandra (8 keV) or is below the minimal value acceptable for the Comptonization model (5 keV (see, for example, [7])). Therefore, the parameter T_s was fixed in three fittings. The Obs.648 spectrum is the only one that shows a very low seed photon temperature: $T_s = 0.020^{+0.004}_{-0.003}$ keV; the presence of many lines in the energy band of this spectrum can affect the parameter value.

The LETG/HRC spectra for SS Cyg and U Gem have not been successfully described by only one thermal Comptonization component. The presence of many lines in the energy range of 0.07–2 keV is challenging for a satisfactory correlation of data. Good agreement in terms of χ^2 statistics is obtained when the band with low energy values ($E < 2.5$ keV in SS Cyg and $E < 1.5$ keV in U Gem) is not taken into account.

4.2.3 Spectral analysis of RXTE. Almost all observations featured a low count rate (< 1 s^{-1}) in the energy range > 25 keV for the PCA spectra and in the range of 40–150 keV for the HEXTE spectra. Therefore, with the exception of Obs.ID 50012-01-01-00 for SS Cyg, the spectral analysis was only carried out for the PCA spectra in the energy range of 3–25 keV. Since the observational data for SS Cyg presented in Fig. 23 were obtained concurrently, they can be studied together.

The spectra of U Gem (Obs.ID 80011-01-02-00), SS Aur (Obs.ID 30026-03-01-00), and SS Cyg (Obs.ID 10040-01-01-000) are well described in the energy range of $\sim 5-25$ keV by only one COMPTT component. On the other hand, three spectra obtained for SS Cyg (Obs.IDs 50012-01-01-00, 10040-01-01-001, and 10040-01-01-00) require the presence of a second spectral component. The applied model consists of the sum of a blackbody and Comptonization components (BBODY + COMPTT) or the sum of two Comptonization (COMPTT + COMPTT) components.

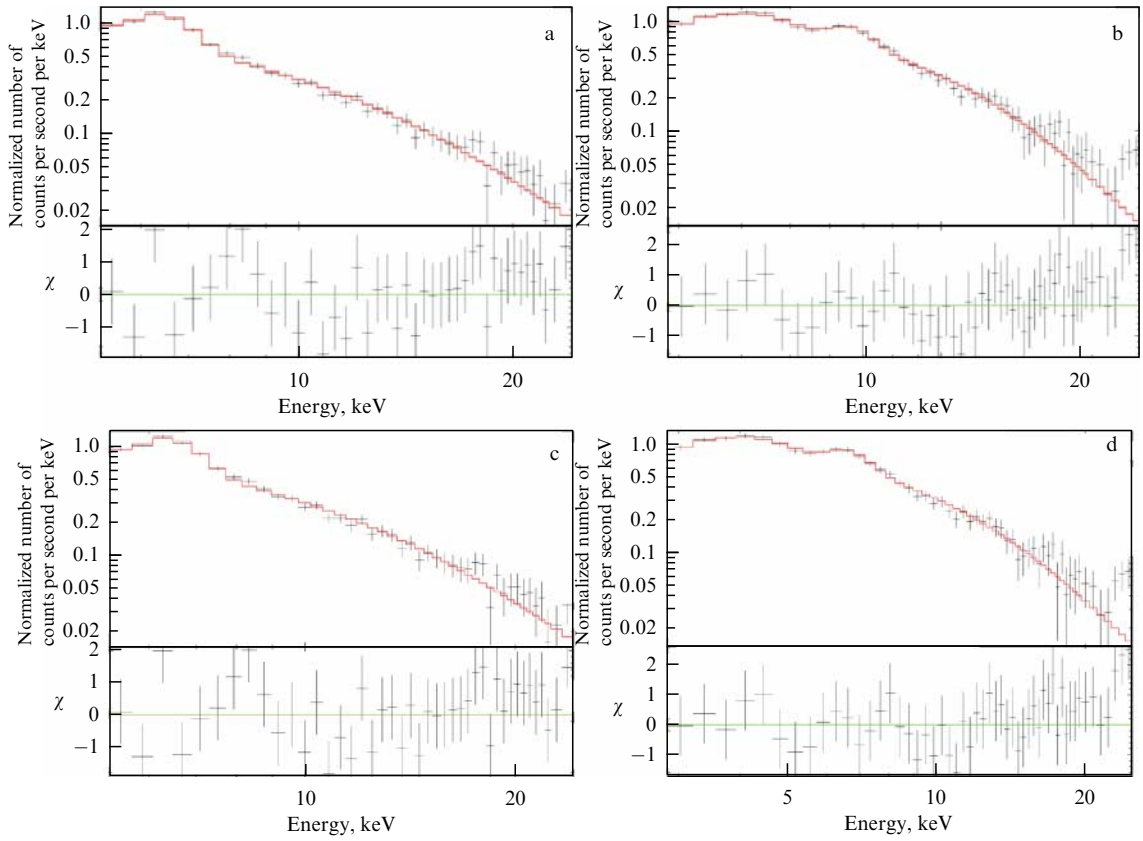

Figure 22. Fitting of model spectra to data obtained by RXTE/PCA for U Gem in the burst state (a) and SS Aur in the quiescent state (b), and for SS Cyg in the burst state: (c) Obs.IDs 10040-01-01-000, (d) Obs.IDs 10040-01-01-001. Red curve represents the COMPTT + GAUSSIAN model. Lower panes of the figures show residual deviations [81].

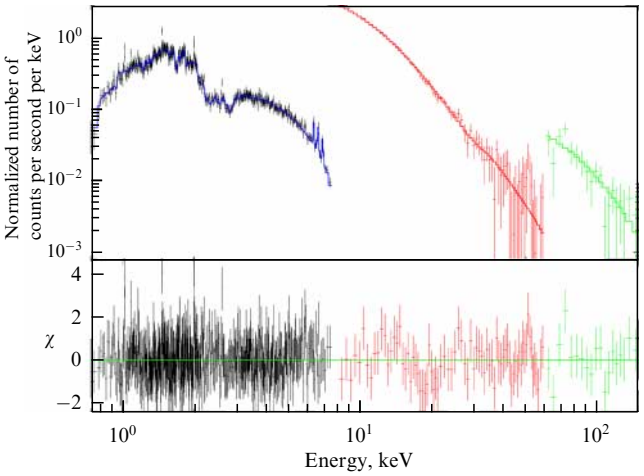

Figure 23. Fitting of the spectrum for simultaneously recorded spectra of SS Cyg obtained in three spectral bands with Chandra/RXTE receivers (Obs.ID 646/Obs.ID 50012-01-01-00). Fitting was carried out using the spectral model COMPTT + COMPTT + GAUSSIAN + GAUSSIAN + GAUSSIAN. Black, red, and green dots correspond to the frequency ranges of 0.4–8.0 keV (HETG/ACIS), 8.0–60 keV (PCA), and 60–150 keV (HEXTE), respectively. Blue, red, and green curves correspond to the best fit. The lower pane of the figure shows the residual deviations of the observational data from the model [81].

Figure 1 shows the general structure of accretion near a compact object, corresponding to the case of Comptonization and sources containing white dwarfs without significant magnetospheres. The observed X-ray spectrum is formed in the transition layer as a result of Comptonization of seed photons emitted from the disk and the WD surface on hot electrons of the Compton cloud. Figure 22 presents the results of spectral fittings for U Gem and SS Aur, and for two observations of the SS Cyg burst. It is of importance to emphasize that these two observations follow each other. Figure 23 displays the result of fitting in the energy range of 0.4–150 keV of the simultaneous spectra of Chandra/RXTE (Chandra HETG/ACIS Obs.ID 646 and RXTE (PCA and HEXTE) Obs.ID 50012-01-01-00) for the quiescent SS Cyg source.

4.3 Constancy of the photon index for cataclysmic variables

Figure 24 shows the relation between the photon index Γ and the electron temperature T_e in the transition layer for all nmCVs. It can be seen in the figure that, for at least 15 nmCV spectra, the observed values of Γ are distributed around a value of 1.8.

4.4 Transition layer and spectral index of the spectrum

As indicated in [15], the release of energy in the transition layer around a neutron star determines the spectral index of the resulting spectrum. Similarly, the transition layer model can be used for white dwarfs. However, in this case, the reflecting inner boundary of the transition layer around the neutron star should be replaced by the boundary of pure absorption. The energy distribution $\varepsilon(\tau)$ can be found as a solution of the diffusion equation in the transition layer. It is also necessary to add two boundary conditions: on the inner

boundary of the transition layer, which is the surface of the white dwarf, $\tau = \tau_0$, and on the outer boundary, $\tau = 0$, respectively:

$$\frac{\mathrm{d}\varepsilon}{\mathrm{d}\tau} + \frac{3}{2}\,\varepsilon\bigg|_{\tau=\tau_0} = 0\,, \tag{23}$$

$$\frac{\mathrm{d}\varepsilon}{\mathrm{d}\tau} - \frac{3}{2}\,\varepsilon\bigg|_{\tau=0} = 0\,. \tag{24}$$

The solution of Eqn (17) with boundary conditions (23) and (24) then takes the form

$$\varepsilon(\tau) = \frac{Q_{\mathrm{cor}}}{c}\left\{1 + \frac{3}{2}\,\tau_0\left[\frac{\tau}{\tau_0} - \left(\frac{\tau}{\tau_0}\right)^2\right]\right\}. \tag{25}$$

Thus, integration of $\varepsilon(\tau)$ yields

$$\int_0^{\tau_0} \varepsilon(\tau)\,\mathrm{d}\tau = \frac{Q_{\mathrm{cor}}}{c}\,\tau_0\left(1 + \frac{\tau_0}{4}\right). \tag{26}$$

Now, using Eqns (16) and (26), we can access the Comptonization parameter Y (see definition in [55]) in the transition layer. Taking into account the intermediate-value theorem, we present Eqn (16) as

$$Q_{\mathrm{cor}} = 20.2\,\hat{T}_{\mathrm{e}}\int_0^{\tau_0} \varepsilon(\tau)\,\mathrm{d}\tau\,, \tag{27}$$

where $\hat{T}_{\mathrm{e}}$ is the average temperature of electrons in the transition layer.

Substituting formula (26) into (27) leads to the following estimate of the Y-parameter in the transition layer:

$$\frac{\hat{T}_{\mathrm{e}}\tau_0(\tau_0/4 + 1)}{m_{\mathrm{e}}c^2} = 0.25\,. \tag{28}$$

As can be seen in Fig. 24, the photon index Γ deviates from 1.8 only insignificantly: namely, for most known sources, $\Gamma = 1.8 \pm 0.1$, and the electron temperature of the Compton cloud varies from 5 to 45 keV. This behavior of the index is similar to that observed in neutron stars [18].

As was pointed out in the classical work [15], the formation of the spectrum in plasma clouds of a finite size

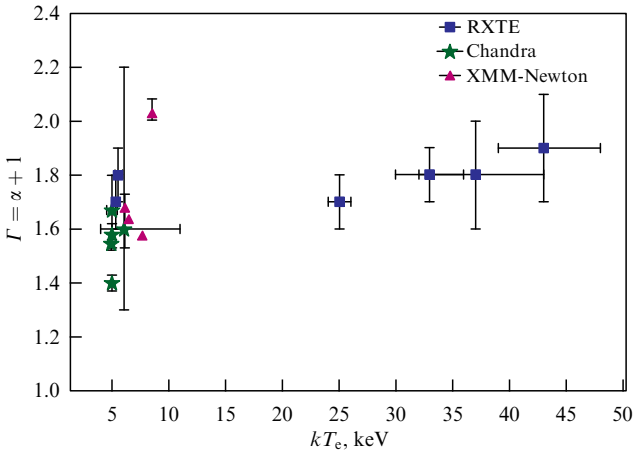

Figure 24. Photon index Γ as a function of plasma temperature T_{e} for various X-ray sources containing a white dwarf. Plateau near $\Gamma = 1.9$ is clearly seen in the entire temperature range (from 5 to 40 keV) [81].

(under conditions of a limited medium) is related to the law of distribution of the number of scatterings that seed photons undergo before escaping. If the average number of photon scatterings is denoted as u_{av} and the dimensionless number of scatterings as $u = N_{\mathrm{e}}\sigma_T ct$, the distribution $u \gg u_{\mathrm{av}}$ is defined as

$$P(u) = A(u, \tau_0)\exp(-\beta u) \tag{29}$$

(see [82]).

For the diffusive regime, when $\tau_0 > 1$, the corresponding value $\beta = \lambda_1^2/3$, where λ_1 is the first eigenvalue of the diffusion operator. According to [82], to find λ_1, it is necessary to solve a differential equation for the intensity of zero momentum,

$$\frac{\mathrm{d}^2 J}{\mathrm{d}\tau^2} + \lambda^2 J = 0\,, \tag{30}$$

with boundary conditions $\mathrm{d}J/\mathrm{d}\tau - (3/2)J = 0$ and $\mathrm{d}J/\mathrm{d}\tau + (3/2)J = 0$ for $\tau = 0$ and $\tau = \tau_0$, respectively. This yields the following formula for the eigenvalue λ_n, $n = 1, 2, 3\ldots$:

$$\tan\left(\frac{\lambda_n\tau_0}{2}\right) = \frac{2}{3\lambda_n}\,, \tag{31}$$

which, in turn, has a solution at $n = 1$:

$$\lambda_1 = \frac{\pi}{2(\tau_0/2 + 2/3)}\,. \tag{32}$$

However, the spectral index α (photon index $\Gamma = \alpha + 1$) is expressed as

$$\alpha = -\frac{3}{2} + \left(\frac{9}{4} + \frac{\beta}{\theta}\right)^{1/2}, \tag{33}$$

where $\beta = \lambda_1^2/3$, $\theta = kT_{\mathrm{e}}/(m_{\mathrm{e}}c^2)$ (see [11]). Thus,

$$\alpha = -\frac{3}{2} + \left(\frac{9}{4} + \frac{\pi^2}{12(\tau_0/2 + 2/3)^2\theta}\right)^{1/2}, \tag{34}$$

wherefrom, using Eqn (28), we obtain $\alpha \lesssim 0.85$ (or $\Gamma \lesssim 1.85$) or exactly what is observed (see [81] and Fig. 24).

4.5 Emission lines and continuum

The total observed emission spectrum consists of a continuum and spectral lines. The emission lines in the spectra of nonmagnetic cataclysmic variables (nmCVs) were analyzed in detail in [81].

Thus, the X-ray continuum is formed in the transition layer in an optically thick medium in the quiescent and burst states. The emission lines appear to be formed in an optically thin region located outside, at a distance both from the transition layer and from the white dwarf surface. Stated differently, the continuum forms closer to the white dwarf than the emission lines do.

Publicly available numerical codes for optically thin thermal plasma and cooling flows make it possible to simultaneously fit continuum and emission lines for several elements and in certain temperature ranges or for several components of optically thin thermal plasma with different temperatures. This approach makes it possible to satisfactorily fit almost all excesses in the spectrum that are superimposed on the continuum. For example, the MEKAL model in the XSPEC package provides an option to simulate 2409 lines for the 15 most important chemical elements (H,

He, C, N, O, Ne, Na, Mg, Al, Si, S, Ar, Ca, Fe, and Ni), and, thus, wide excesses over the continuum can be approximated by a few narrow emission lines. Alterations concerning the description of the continuum based on the Comptonization model make it possible to determine the residual excesses in the spectra (i.e., to detect emission lines) observed immediately after the simulation of the continuum, as is done for low-mass X-ray binaries (LMXBs). In this case, each of the emission lines should be independently determined by modeling the Gaussian components. Using the thermal Comptonization component (COMPTT or COMPTB) to approximate the continuum in the nmCV, the authors of [81] successfully identified a broad strong emission line peaking at $\sim 0.96-1.02$ keV in all analyzed spectra obtained by XMM-Newton in the range of $\sim 0.8-1.2$ keV using one Gaussian.

It is of importance to emphasize that the indicated wide excess over the continuum should most likely be described as a mixture of narrow lines emitted by Fe XVII, XIX, XX, and XXI, Ne IX–X, and/or Ni XIX ions, which are not very well resolved by the pn-camera and HETG/ACIS. Several lines were observed in the indicated X-ray range by the LETG/HRC spectrometer (due to its resolution of > 1000) (see also, e.g., [83, 84]). In the analysis carried out in [81] for SS Cyg based on the data obtained by LETG/HRC, the lines at energies of ~ 0.82, ~ 0.92, and ~ 1.0 keV are clearly presented.

4.6 Discussion

As mentioned earlier, the Comptonization model is not the standard model currently used to describe the continuum in nmCVs. On the other hand, the Comptonization model is the standard for fitting LMXB spectra.

Given that nmCPs are similar to LMXBs, i.e., such a stellar system has an accretion disk, a compact object, and a transition layer (corona), the presence of which is evident from the observation of uneclipsed ultraviolet emission lines in eclipsing systems (see, for example, [85, 86]), it is logical to assume that a spectral similarity should exist between these two types of X-ray binaries.

All sources in the sample analyzed in [81] were observed in the quiescent state using the XMM-Newton Epic-pn. It was found that, to describe the spectra of two nmCVs, SS Cyg and SS Aur, one thermal Comptonization component supplemented with Gaussian components is sufficient. In terms of χ^2-statistics, the model failed to provide an ideal description of the full spectra of VW Hyi and U Gem XMM-Newton. In the last two cases, χ^2 exceeds the critical value at a significance level of 0.01. Nevertheless, the spectral analysis of U Gem using Chandra and RXTE data exhibits satisfactory agreement. Probably, the presence of several emission lines, in addition to iron lines, in the XMM-Newton spectra for VW Hyi and U Gem deteriorated the quality of the fit.

It is important to emphasize that all XMM-Newton spectra show that the best fit of the model to observations is attained with the following values of the parameters: average seed photon temperature $\langle T_s \rangle = 0.15 \pm 0.01$ keV, average optical depth 4.11 ± 0.27, and average electron temperature in the Compton cloud $T_e = 7.19 \pm 0.16$ keV. The model was fitted to the observed spectra in the energy range of 1.5–15 keV (for XMM-Newton), so the temperature of seed photons T_s could not be accurately estimated. In this case, the average values of the parameters were fixed: $\langle T_s \rangle = 0.25 \pm 0.03$ keV, $\langle T_e \rangle = 5.93 \pm 0.16$ keV, and $\langle \tau \rangle = 4.5 \pm 0.3$.

The Chandra HETG/ACIS spectra show parameter values similar to those found for the XMM-Newton data, with an average seed photon temperature of 0.20 ± 0.09 keV, an average optical depth $\tau = 5.2 \pm 0.1$, and an average electron temperature $T_e = 5.78 \pm 0.29$ keV. SS Cyg was observed once in the quiescent state and twice in a burst state. However, the analysis carried out in [81] failed to provide an ideal match for two observations in the burst. In addition, the spectral continuum parameters do not differ between the two states, which may be due to Chandra's effective energy band (< 8 keV).

In analyzing the RXTE spectra, a second Comptonization component is needed to describe the full spectrum in three observations of SS Cyg. In these cases, a satisfactory fit to the spectrum was found if these two components, and the optical depth τ of the COMPTT model, were linked via T_e, implying that the total spectra of the ranges 0.4–150 keV or 2.5–25 keV of all analyzed nmCVs are characterized by only one spectral index, α.

The RXTE spectra of the presented sample showed that the electron temperature range is very wide, 5–48 keV. Therefore, in looking for correlations, T_e cannot be established (see [81]). It is worth noting that SS Cyg exhibits $T_e \sim 5$ keV during a burst, U Gem, 43^{+5}_{-4} keV (also in the burst state), and SS Aur in the quiescent state, 37^{+6}_{-5} keV.

In the RXTE spectra, the average seed photon temperature of the first Comptonization component is $T_{s1} = 0.20 \pm 0.04$ keV. The temperature T_{s1} appears in the burst observations described above. SS Cyg shows that T_{s1} is approximately two to three times higher when the source is in a burst state. Note, however, that the RXTE data do not accurately determine the seed photon temperatures if these temperatures are much less than 1 keV, since the lower limit of the RXTE data lies near 3 keV. Therefore, the seed photon temperature T_s obtained from the RXTE data is only an upper limit.

In the Comptonization model, all seed photons gain energy on hot electrons of a Compton cloud surrounding a compact object [11]. The analysis carried out in [81] showed that the nmCV contains up to two components of seed photons, presumably coming from the inner and outer parts of the transition layer with color temperatures T_{s1} and T_{s2}, while Comptonization of both components occurs in the transition layer located between the surface of the white dwarf and the inner part of the accretion disk. The electrons in the transition layer are characterized by one value of temperature, which is clearly seen from the analysis of the RXTE spectra.

The source of hard X-rays in the spectral quiescent state is compact, which is confirmed by the light curves of eclipsing dwarf novae [5, 87]. Therefore, the hot Comptonization cloud (transition layer) should also be compact. One photon component, featuring the lowest temperatures ($T_{s1} \sim 0.1$–0.2 keV), comes from the interior of the accretion disk, while the other, with temperature T_{s2}, comes from the inner part of the system, much closer to the WD surface or directly from it.

Accounting for interstellar absorption for the studied sources yields lower temperatures. If the interstellar absorption parameter, N_H, is fixed at the value expected for the direction to the source, in the XMM-Newton spectra for the sources VW Hyi, U Gem, and SS Aur, the temperature T_{s1} takes values of ~ 0.01 keV, but, in addition to the observed increase in χ^2_{red}, this parameter was not significantly limited by the fit. The same result was obtained when N_H was set as a free

parameter: in some cases, it took a very small value, equal to 10^{19} atoms cm^{-2}, and did not affect the values of the parameters in any approximation.

Figure 23 shows the quiescent spectrum of SS Cyg in the energy range of 0.4–150 keV. The spectrum corresponds to the simultaneous observations of Chandra HETG/ACIS Obs.ID 646 and RXTE (PCA and HEXTE) ID 50012-01-01-00. It is of importance to note that spectral analysis, which also takes into account data in the hard X-ray range (> 15 keV), is of significance for constraining the physical parameters. In this case, for example, the electron temperature in the transition layer is 33^{+3}_{-3} keV, and the spectral index $\Gamma = 1.8^{+0.1}_{-0.1}$. If the analysis only includes the HETG/ACIS spectrum, we arrive at smaller values: $T_e = 5$ keV and $\Gamma = 1.55^{+0.02}_{-0.03}$.

A possible change in the spectral description of cataclysmic variables (from an optically thin thermal plasma to the scattering of soft photons with an increase in their frequency due to the inverse Compton effect in a thick Comptonization cloud) is similar to the adoption of the Comptonization model for describing LMXB spectra in the energy range of $\sim 3-50$ keV, because, prior to the general recognition of Comptonization, the mechanism employed to describe the LMXB spectra was bremsstrahlung (see, for example, [88]). Similarly, bremsstrahlung is a radiative process based on the MEKAL and cooling flow models that have been used to match the spectral continuum of cataclysmic variables. In LMXB, the use of the Comptonization model was subsequently extended to a wider (from ~ 0.3 keV to ~ 250 keV) band [18, 73, 89, 90].

As shown in Fig. 24, the observed photon indices Γ are distributed around 1.8 according to data for at least 15 nmCVs. In addition, in Section 4.4, the photon index of the spectrum formed in the transition layer around a WD was theoretically estimated. For this purpose, the radiative transport formalism was applied to solve the boundary value problem for the energy density distribution in the transition layer around a white dwarf (see (25)) and the release Q of gravitational energy in the transition layer was estimated (see (27)) to find the Comptonization parameter represented by Eqn (28). Moreover, the solution to the eigenvalue problem for the average intensity $J(\tau)$ (see (30)) and the use of Eqn (33) for the spectral index α, combined with estimate (28), lead to the unambiguous conclusion that the photon index in the transition layer of an accreting white dwarf should be about 1.85. This is the first fundamental estimate of the photon index, which is indeed confirmed by the presented analysis of nmCV observations.

4.7 Conclusions

The thermal Comptonization model supplemented with Gaussian components to take into account radiation in lines can successfully describe nmCV spectra. In terms of χ^2 statistics, the spectra of the considered nmCVs satisfactorily agree with the Comptonization model. The presence of many lines, in addition to the lines of the iron complex, in the VW Hyi and U Gem spectra has probably deteriorated the quality of the fit.

The spectra of sources obtained in various energy ranges (XMM-Newton and Chandra) exhibit a similar range of physical parameters. However, the RXTE spectra, due to a wider energy range, provided a better description of the Comptonization effect and determination of the physical parameters. For example, it was found in [81] that successful matching of the simultaneous Chandra/RXTE spectra of quiescent SS Cyg in the 0.4–150 keV energy range and two RXTE burst spectra of SS Cyg in the 2.5–25 keV energy range requires two Comptonization components. In this case, the best matches were only obtained when the optical depth and plasma temperature of the Compton cloud were the same for both of these components. It was shown as a result that a single value of the photon index Γ with a value close to 1.8 is sufficient to describe the total spectrum of all analyzed nmCVs.

The two blackbody components of the seed photons are characterized by color temperatures T_{s1} and T_{s2}. In our interpretation, the initial photon component, exhibiting the lowest temperatures, T_{s1}, presumably comes from the interior of the accretion disk (or the outer part of the transition layer), while the second transition component, with temperature T_{s2}, arrives from deeper layers of the system, closer to the WD surface. Apparently, these temperatures are associated with the innermost part of the corona (transition layer).

Seed photons, regardless of their source, are Comptonized by hot electrons located between the accretion disk and the white dwarf surface of the transition layer characterized by a single electron temperature T_e, which for the studied systems lies in the range of 5–48 keV. The optical thickness of the transition layer varies over a wide range, $1 \lesssim \tau \lesssim 5$.

In comparing the physical parameters of various sources in different states, no correlation has been observed between the photon index and the plasma temperature T_e (see Fig. 24). However, RXTE observations of SS Cyg unambiguously show that the electron temperature in a Compton cloud (or the transition layer) changes depending on the state of the X-ray source: T_e is higher is the quiescent state, 33^{+3}_{-3} keV; at the initial stage of the optical burst, it decreases to 25^{+1}_{-1} keV to drop to $5.5^{+0.4}_{-0.3}$ keV during the burst. This decrease in the electron temperature can be explained by the suppression of hard X-rays ($\gtrsim 25$ keV) during the burst in SS Cyg.

Thus, the two-component Comptonization model, which employs one value of the thermal plasma temperature and one value of the optical depth, and is supplemented by Gaussian components to describe the emission in lines, can describe the nmCV spectra in a wide energy range (0.4–150 keV) both in the quiescent and burst states.

5. Conclusions

One of the trends in modern astrophysics has been the emergence of multi-wave astronomy, which uses for studying physical objects — stars and galaxies — data obtained in various wavelength ranges. These data complement each other, making it possible to more accurately and clearly understand the picture of physical processes. The next stage of development in this area is multi-messenger astronomy, when data from neutrino installations and gravitational-wave detectors (interferometers) can be used for complex analysis.

The unity of physics at different scales makes it possible to describe 'from first principles' the phenomena occurring on different scales, such as accretion flows near the event horizon of astrophysical and supermassive BHs. Based on the scaling technique originally developed for X-ray binaries, it is possible to develop an independent method for determining the mass of supermassive black holes in active galactic nuclei and black holes of intermediate masses. The option that has emerged seems especially interesting in our time, when the

success of radio interferometry has made it possible for the first time to directly 'see' the black hole shadow.

Over the past half century, black holes have turned from an almost peculiar solution of the equations of General Relativity (GR) into an ordinary astrophysical object, which potentially provides options for testing the relativistic theory of gravity in strong gravitational fields. Black holes, in all the diversity of their manifestations — from microscopic, evaporating in the present era, to supermassive, maintaining the activity of galactic nuclei — provide researchers with such an opportunity.

The increasing flow of observational data and the need for their reconciliation naturally lead to the complicating of both physical models and the corresponding magnetohydrodynamic calculations, which require taking into account the effects of General Relativity. However, the construction of simple physical models of radiation sources remains of importance. The X-ray formation model considered in this review, which was proposed more than 20 years ago, successfully explains the main spectral features of X-ray emission from black holes, neutron stars, and white dwarfs without significant magnetospheres.

The list of these features includes the correlation of the spectral index with the frequency of quasi-periodic oscillations in the range of 1–10 Hz for black holes with masses on the order of several solar ones. For X-ray sources with neutron stars, the photon index remains almost constant, about 2. In the case of white dwarfs, the photon index also varies slightly, but near another value, 1.85. This characteristic behavior of the photon index is a distinctive feature of each type of compact source.

Acknowledgments

The authors are grateful to the referee for their constructive comments, which helped to improve the text of the review. L G T highly appreciates the interest and support of his colleagues from the Lebedev Physical Institute of the Russian Academy of Sciences.

References

1. Titarchuk L, Lapidus I, Muslimov A *Astrophys. J.* **499** 315 (1998)
2. Patterson J, Raymond J C *Astrophys. J.* **292** 550 (1985)
3. Patterson J, Raymond J C *Astrophys. J.* **292** 535 (1985)
4. Williams G A, King A R, Brooker J R E *Mon. Not. R. Astron. Soc.* **226** 725 (1987)
5. Mukai K *Publ. Astron. Soc. Pac.* **129** 062001 (2017)
6. Titarchuk L *Astrophys. J.* **434** 570 (1994)
7. Hua X-M, Titarchuk L *Astrophys. J.* **449** 188 (1995)
8. Titarchuk L, Lyubarskij Y *Astrophys. J.* **450** 876 (1995)
9. Farinelli R et al. *Astrophys. J.* **680** 602 (2008)
10. Montanari E, Titarchuk L, Frontera F *Astrophys. J.* **692** 1597 (2009)
11. Sunyaev R A, Titarchuk L G *Astron. Astrophys.* **86** 121 (1980)
12. Ivanov P B et al. *Phys. Usp.* **62** 423 (2019); *Usp. Fiz. Nauk* **189** 449 (2019)
13. Shaposhnikov N, Titarchuk L *Astrophys. J.* **699** 453 (2009)
14. Titarchuk L et al. *Astron. Astrophys.* **633** A73 (2020)
15. Farinelli R, Titarchuk L *Astron. Astrophys.* **525** 102 (2011)
16. Seifina E, Titarchuk L *Astrophys. J.* **738** 128 (2011)
17. Maiolino T et al. *Astrophys. J.* **911** 80 (2021)
18. Titarchuk L, Seifina E, Shrader C *Astrophys. J.* **789** 98 (2014)
19. Belloni T *AIP Conf. Proc.* **797** 197 (2005)
20. Remillard R A, McClintock J E *Annu. Rev. Astron. Astrophys.* **44** 49 (2006)
21. Klein-Wolt M, van der Klis M *Astrophys. J.* **675** 1407 (2008)
22. Shaposhnikov N, Titarchuk L *Astrophys. J.* **643** 1098 (2006)
23. Titarchuk L, Fiorito R *Astrophys. J.* **612** 988 (2004)
24. Shaposhnikov N, Titarchuk L *Astrophys. J.* **663** 445 (2007)
25. Miller-Jones J C A et al. *Science* **371** 1046 (2021)
26. Dewangan G C, Titarchuk L, Griffiths R E *Astrophys. J.* **637** L21 (2006)
27. Dewangan G C, Griffiths R E, Rao A R *Astrophys. J.* **641** L125 (2006)
28. Strohmayer T E et al. *Astrophys. J.* **660** 580 (2007)
29. Revnivtsev M, Gilfanov M, Churazov E *Astron. Astrophys.* **363** 1013 (2000)
30. Titarchuk L, Mastichiadis A, Kylafis N D *Astrophys. J.* **487** 834 (1997)
31. Dickey J M, Lockman F J *Annu. Rev. Astron. Astrophys.* **28** 215 (1990)
32. Laurent P, Titarchuk L *Astrophys. J.* **511** 289 (1999)
33. Shakura N I, Sunyaev R A *Astron. Astrophys.* **24** 337 (1973)
34. Titarchuk L, Zannias T *Astrophys. J.* **493** 863 (1998)
35. Laurent P, Titarchuk L *Astrophys. J.* **727** 34 (2011)
36. Greene J, Bailyn C D, Orosz J A *Astrophys. J.* **554** 1290 (2001)
37. Hjellming R M, Rupen M P *Nature* **375** 464 (1995)
38. Muños-Darias T, Casares J, Martínes-Pais I G *Mon. Not. R. Astron. Soc.* **385** 2205 (2008)
39. Hynes R I et al. *Astrophys. J.* **609** 317 (2004)
40. Orosz J A, in *A Massive Star Odyssey: from Main Sequence to Supernova. Proc. of IAU Symp. No. 212, 24–28 June 2001, Spain* (Eds K van der Hucht, A Herrero, C Esteban) (San Francisco: Astron. Soc. of the Pacific, 2003) p. 365
41. Park S Q et al. *Astrophys. J.* **610** 378 (2004)
42. Orosz J A et al. *Astrophys. J.* **568** 845 (2002)
43. Sánchez-Fernández C et al. *Astron. Astrophys.* **348** L9 (1999)
44. Sobczak G J et al. *Astrophys. J.* **517** L121 (1999)
45. Orosz J A et al. *Astrophys. J.* **616** 376 (2004)
46. Homan J et al. *Mon. Not. R. Astron. Soc.* **366** 235 (2006)
47. McClintock J E et al. *Astrophys. J.* **698** 1398 (2009)
48. Filippenko A V, Chornock R *IAU Circ.* **7644** 2 (2001)
49. Zurita C et al. *Mon. Not. R. Astron. Soc.* **334** 999 (2002)
50. Herrero A et al. *Astron. Astrophys.* **297** 556 (1995)
51. Ninkov Z, Walker G A H, Yang S *Astrophys. J.* **321** 425 (1987)
52. Titarchuk L et al. *Astrophys. J.* **560** L55 (2001)
53. Titarchuk L, Shaposhnikov N *Astrophys. J.* **678** 1230 (2008)
54. Laurent P, Titarchuk L *Astrophys. J.* **656** 1056 (2007)
55. Rybicki G B, Lightman A P *Radiative Processes in Astrophysics* (New York: Wiley, 1979) p. 46
56. Titarchuk L, Seifina E *Astron. Astrophys.* **595** A101 (2016)
57. Titarchuk L, Seifina E *Astron. Astrophys.* **585** A94 (2016)
58. Seifina E, Chekhtman A, Titarchuk L *Astron. Astrophys.* **613** A48 (2018)
59. Seifina E, Titarchuk L, Ugolkova L *Astron. Astrophys.* **619** A21 (2018)
60. Event Horizon Telescope Collab. *Astrophys. J. Lett.* **930** 12E (2022)
61. Titarchuk L, Seifina E *Mon. Not. R. Astron. Soc.* **501** 5659 (2021)
62. Rhoades C E (Jr.), Ruffini R *Phys. Rev. Lett.* **32** 324 (1974)
63. Seifina E, Titarchuk L, Shaposhnikov N *Astrophys. J.* **821** 23 (2016)
64. Seifina E et al. *Astrophys. J.* **808** 142 (2015)
65. Seifina E, Titarchuk L, Frontera F *Astrophys. J.* **766** 63 (2013)
66. Titarchuk L, Seifina E, Frontera F *Astrophys. J.* **767** 160 (2013)
67. Seifina E, Titarchuk L *Astrophys. J.* **747** 99 (2012)
68. Di Salvo T et al. *Astrophys. J.* **542** 1034 (2000)
69. Piraino S, Santangelo A, Kaaret P *Astron. Astrophys.* **360** L35 (2000)
70. D'Ai A et al. *Astron. Astrophys.* **448** 817 (2006)
71. Ng C et al. *Astron. Astrophys.* **522** A96 (2010)
72. Egron E et al. *Astron. Astrophys.* **530** A99 (2011)
73. Di Salvo T et al. *Astrophys. J. Lett.* **649** L91 (2006)
74. Titarchuk L, Shaposhnikov N *Astrophys. J.* **724** 1147 (2010)
75. Di Salvo T et al. *Astrophys. J.* **546** 1107 (2001)
76. Zel'dovich Ya B, Shakura N I *Sov. Astron.* **13** 175 (1969); *Astron. Zh.* **46** 225 (1969)
77. Bisnovatyi-Kogan G S et al. *Sov. Astron.* **24** 716 (1980); *Astron. Zh.* **57** 1242 (1980)
78. Titarchuk L, Seifina E *Astrophys. J.* **706** 1463 (2009)

79. Seifina E, Titarchuk L *Astrophys. J.* **722** 586 (2010)
80. Soria R et al. *Mon. Not. R. Astron. Soc.* **410** 1886 (2011)
81. Maiolino T et al. *Astrophys. J.* **900** 153 (2020)
82. Sunyaev R A, Titarchuk L G *Astron. Astrophys.* **143** 374 (1985)
83. Mukai K et al. *Astrophys. J. Lett.* **586** L77 (2003)
84. Pandel D, Córdova F A, Howell S B *Mon. Not. R. Astron. Soc.* **346** 1231 (2003)
85. Warner B *Cataclysmic Variable Stars* (Cambridge Astrophysics Series, Vol. 28) (Cambridge: Cambridge Univ. Press, 1995)
86. Mauche C W, Raymond J C *Astrophys. J.* **541** 924 (2000)
87. Lewin W, van der Klis M (Eds) *Compact Stellar X-ray Sources* (Cambridge Astrophysics Ser., Vol. 39) (Cambridge: Cambridge Univ. Press, 2006)
88. D'Amico F et al. *Astrophys. J.* **547** L147 (2001)
89. D'Aí A et al. *Astrophys. J.* **667** 411 (2007)
90. Maiolino T, D'Amico F, Braga J *Astrophys. J.* **551** L2 (2013)